Title

A diet-dependent host metabolite shapes the gut microbiota to protect from autoimmunity.

Journal

Cell Reports, 43(11)

Authors

Alexander, Margaret
Upadhyay, Vaibhav
Rock, Rachel
et al.

Publication Date

2024-11-26

DOI

10.1016/j.celrep.2024.114891

Peer reviewed

HHS Public Access

Author manuscript

Cell Rep. Author manuscript; available in PMC 2024 December 20.

Published in final edited form as:

Cell Rep. 2024 November 26; 43(11): 114891. doi:10.1016/j.celrep.2024.114891.

A diet-dependent host metabolite shapes the gut microbiota to protect from autoimmunity

Margaret Alexander[1,2], **Vaibhav Upadhyay**[1,3], **Rachel Rock**[1], **Lorenzo Ramirez**[1], **Kai Trepka**[1], **Patrycja Puchalska**[4], **Diego Orellana**[3], **Qi Yan Ang**[1], **Caroline Whitty**[1], **Jessie A. Turnbaugh**[1], **Yuan Tian**[5], **Darren Dumlao**[3], **Renuka Nayak**[3,6], **Andrew Patterson**[5], **John C. Newman**[7,8], **Peter A. Crawford**[4,9], **Peter J. Turnbaugh**[1,10,11,*]

[1]Department of Microbiology & Immunology, University of California, San Francisco, San Francisco, CA 94143, USA

[2]Department of Medical Microbiology and Immunology, University of Wisconsin – Madison, Madison, WI 53706, USA

[3]Department of Medicine, University of California, San Francisco, San Francisco, CA 94158, USA

[4]Division of Molecular Medicine, University of Minnesota, Minneapolis, MN 55455, USA

[5]Department of Veterinary and Biomedical Sciences, Pennsylvania State University, University Park, PA 16802, USA

[6]San Francisco VA Medical Center, San Francisco, CA 94121, USA

[7]Buck Institute for Research on Aging, Novato, CA 94945, USA

[8]Division of Geriatrics, University of California, San Francisco, San Francisco, CA 94158, USA

[9]Department of Biochemistry, Molecular Biology, and Biophysics, University of Minnesota, Minneapolis, MN 55455, USA

[10]Chan Zuckerberg Biohub – San Francisco, San Francisco, CA 94158, USA

[11]Lead contact

SUMMARY

*Correspondence: peter.turnbaugh@ucsf.edu.

AUTHOR CONTRIBUTIONS

Conceptualization: M.A. and P.J.T.; data curation: M.A., V.U., L.R., R.R., and K.T.; formal analysis: M.A. and V.U.; funding acquisition: R.N., M.A., P.J.T., and J.C.N.; investigation: M.A., V.U., and Q.Y.A.; methodology: M.A., V.U., Q.Y.A., P.P., P.A.C., R.R., D.O., L.R., J.A.T., and C.W.; project administration: P.J.T.; resources: P.J.T., P.A.C., and J.C.N.; software: V.U.; supervision: P.J.T., R.N., J.C.N., P.A.C., and A.P.; validation: M.A. and V.U.; visualization: M.A. and V.U.; writing – original draft: M.A.; writing – review & editing: P.J.T.

DECLARATION OF INTERESTS

P.J.T. is on the scientific advisory boards for Pendulum, Seed, and SNIPRbiome; there is no direct overlap between the current study and these consulting duties. P.A.C. has served as an external consultant for Pfizer, Inc., Abbott Laboratories, Janssen Research & Development, and Selah Therapeutics. J.C.N. is scientific co-founder and stockholder for BHB Therapeutics (which provided the ketone ester) and Selah Therapeutics.

SUPPLEMENTAL INFORMATION

Supplemental information can be found online at https://doi.org/10.1016/j.celrep.2024.114891.

Diet can protect from autoimmune disease; however, whether diet acts via the host and/or microbiome remains unclear. Here, we use a ketogenic diet (KD) as a model to dissect these complex interactions. A KD rescued the experimental autoimmune encephalomyelitis (EAE) mouse model of multiple sclerosis in a microbiota-dependent fashion. Dietary supplementation with a single KD-dependent host metabolite (β-hydroxybutyrate [βHB]) rescued EAE, whereas transgenic mice unable to produce βHB in the intestine developed more severe disease. Transplantation of the βHB-shaped gut microbiota was protective. *Lactobacillus* sequence variants were associated with decreased T helper 17 cell activation *in vitro*. Finally, we isolated an *L. murinus* strain that protected from EAE, which was phenocopied by a *Lactobacillus* metabolite enriched by βHB supplementation, indole lactate. Thus, diet alters the immunomodulatory potential of the gut microbiota by shifting host metabolism, emphasizing the utility of taking a more integrative approach to study diet-host-microbiome interactions.

Graphical abstract

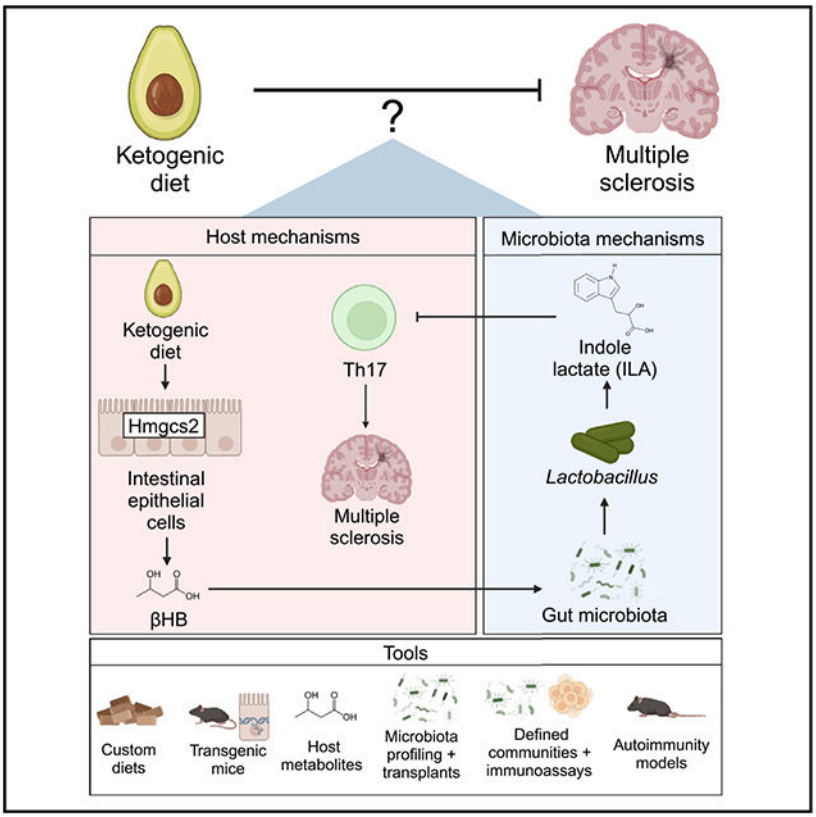

In brief

Identifying the optimal diet for patients suffering from autoimmune disease remains challenging. Here, Alexander and colleagues dissect the complex host-microbiome interactions, explaining the protective effects of a ketogenic diet for a mouse model of neuroinflammation. They highlight the importance of host β-hydroxybutyrate and bacterial indole lactate, inspiring more precise interventions.

INTRODUCTION

Diet has broad impacts on autoimmune disease, including multiple sclerosis (MS), inflammatory bowel disease, and rheumatoid arthritis,[1–5] but the mechanisms responsible remain unclear. Consumption of a high-fat, low-carbohydrate ketogenic diet (KD) improves MS-related symptoms in humans[6–8] and mice.[9–11] KDs are defined by a metabolic shift in host metabolism to lipid oxidation, resulting in elevated concentrations of the ketone bodies β-hydroxybutyrate (βHB) and acetoacetate (AcAc) in circulation.[12] AcAc and βHB have broad impacts on immune cells, acting to dampen inflammasome activation,[13] alter macrophage metabolism,[14] and promote T cell function,[15] among other immunomodulatory effects,[12] providing a direct link between diet-induced shifts in host metabolites and the immune system.

KDs can also indirectly shape the immune system by altering the trillions of microorganisms that colonize the gastrointestinal (GI) tract (the gut microbiota) and/or their aggregate genomes and metabolic activities (the gut microbiome).[16–19] KD-induced shifts in the gut microbiotas of humans and mice result in decreased intestinal immune activation, in part due to the direct antimicrobial properties of βHB.[16] Yet the relevance of these diet-induced shifts in the gut microbiota for disease, especially diseases outside the gut, have remained unknown. Due to the complex interactions of KDs on the host and microbiota, our goal was to gain mechanistic insights that would enable the development of more targeted interventions in future studies.

Here, we dissect the role of diet in shaping host-microbiome interactions relevant to disease. We chose to focus on the experimental autoimmune encephalomyelitis (EAE) mouse model for multiple reasons. The EAE model has been widely used in the autoimmunity field,[20,21] is microbiota dependent,[22] and can be readily performed in gnotobiotic mice.[23] While human MS differs in many ways from EAE,[21] multiple MS-associated microorganisms exacerbate the EAE phenotype,[22–24] and transplantation of the gut microbiota from MS patients increases disease in the EAE model relative to healthy controls.[23,25] These results indicate that aspects of EAE reflect clinically relevant host-microbiome interactions, providing mechanistic insights essential to interpreting the large-scale studies correlating aspects of the gut microbiome with MS in patients.[26]

We identify a pathway through which a microbial community shaped by intestinal production of βHB protects from EAE disease. By pairing recently described methods for generating stable *in vitro* communities[27] with a T helper 17 (Th17) skewing assay, we identify and isolate an immunomodulatory member of the *Lactobacillus murinus* species from a mouse fed the KD. This strain and its metabolite indole-3-lactate (ILA) were sufficient to decrease immune activation and ameliorate the EAE phenotype. These results provide new targets for therapeutic manipulation and a foundation to explore the mechanistic links between host and microbial metabolism in response to defined dietary perturbations.

RESULTS

The impact of diet on neurological phenotypes is microbiota dependent

First, we sought to confirm that a KD protects conventionally raised (CONV-R) mice from EAE.[9,10] We fed 12-week-old female C57BL/6J CONV-R mice a high-fat diet (HFD, 75%:15%:10% fat:carbohydrate:protein) or a matched-ingredient KD (90.5%:0%:9.5% fat:carbohydrate:protein; Table S1). Our diets were formulated to control for ingredient differences that have confounded previous comparisons of semi-purified KDs and the more complex chow diet.[9–11,16,28,29] As expected, the KD led to significantly increased circulating βHB relative to HFD controls (Figure S1A). Ten days after diet initiation, we induced EAE via immunization with a myelin oligodendrocyte glycoprotein (MOG) peptide. Disease was assessed by four commonly used metrics[22,24,30]: (1) disease score over time; (2) the rate of disease incidence; (3) the maximum disease developed; and (4) the distribution of mice across maximum disease scores.

The KD significantly reduced disease severity. While HFD mice gradually increased in disease score over 28 days, the KD group had lower disease severity over time (Figure 1A). The incidence rate for the HFD group was 60% compared to 40% in the KD group (Figure 1B), with an average maximum disease score of diseased mice of 3.81 ± 0.38 compared to 2.68 ± 0.63 in the KD group (Figures 1C and 1D). These symptoms were consistent with flow-cytometry-based analyses of immune cells in the brain and spleen 16 days post immunization at peak disease. KD-fed mice had significantly lower $CD4^+$ helper T cells co-producing interferon-γ (IFNγ) and interleukin-17a (IL-17a) in the brain and spleen, which have been previously implicated in EAE[31] (Figures 1E–1H and S1B–S1D). KD-fed mice also had decreased disease severity compared to mice on a chow diet in an independent experiment (Figure S1E). Together with prior data from the intestine of healthy mice,[16] these results indicate that the impact of the KD on immune activation extends beyond the GI tract to alter systemic immunity and are consistent with previous findings that KDs are protective in MS.[9–11]

Next, we sought to test whether the protective effect of a KD during EAE is dependent on the microbiota. We repeated the same dietary intervention using 9- to 12-week-old C57BL/6J female germ-free (GF) mice (n = 11–12 mice/group; four cages per isolator; two independent experiments). Mice were fed an HFD or KD prior to EAE induction and monitored for 25 days. Serum βHB was significantly elevated in GF KD-fed mice relative to HFD (Figure S1F). In contrast to CONV-R mice (Figures 1A–1D), there were no significant differences between GF mice fed HFD and KD across any of the four disease metrics (Figures 1I–1L). Consistent with prior work,[22] GF mice on the HFD had significantly decreased disease phenotypes relative to HFD-fed CONV-R mice (Figure S1G). Thus, the microbiota alters both the initiation of disease and the protective effect of a KD.

Intestinal βHB is necessary and sufficient to protect from disease

The dietary shift to a KD has broad implications for host and microbial metabolism that could feasibly alter the immune system.[32] We opted to focus on the ketone body βHB (Figure 2A) given its dependence on the KD and prior links to both immune cells[33–35] and

the microbiota.[16] We supplemented the HFD with a βHB-containing ketone ester (100 g/kg hexanoyl hexyl β-hydroxybutyrate, C6x2-βHB, Table S1), which leads to increased gut and circulating βHB.[16] We fed 12-week-old CONV-R male and female C57BL/6J mice an HFD, HFD-KE, or KD for 3 days prior to EAE disease induction, and disease was tracked for 21 days.

Remarkably, pharmacological administration of βHB ketone ester (βHB-KE) effectively protected mice from EAE. As previously observed,[16,36] βHB-KE and KD both increased circulating βHB levels (Figure 2B). Consistent with our earlier findings (Figure 1A), the HFD group had significantly increased disease scores over time compared to the KD group (Figure 2C). The HFD-KE group was indistinguishable from KD by either disease score (Figure 2C) or incidence rate (Figure 2D). Maximum disease scores were markedly lower in HFD-KE (0.75 ± 0.14) and KD (1.10 ± 0.37) relative to HFD (4.08 ± 0.66, Figure 2E), with all HFD-KE mice scoring ≤2 (Figure 2F). Additionally, both KD and HFD-KE were protective in a relapsing-remitting EAE model in SJL/J mice with proteolipid protein (PLP),[37,38] showing reduced disease scores, similar incidence rates, and decreased maximum disease scores compared to HFD-fed mice (Figures 2G–2J). Thus, βHB-KE supplementation is sufficient to improve EAE disease severity.

Although βHB was delivered orally through the diet, it could potentially exert an impact on EAE directly in the central nervous system or in other tissues following absorption from the GI tract. To assess whether intestinal production of βHB is required for the full protective effect of a KD, we generated and validated a transgenic mouse model to selectively abolish the intestinal production of βHB (Figure S2). 3-Hydroxy-3-methylglutaryl-CoA synthase 2 (HMGCS2) is the rate-limiting enzyme for βHB production and is highly expressed in intestinal epithelial cells (IECs) within the large intestine.[39] We generated *Hmgcs2*^{WT} (*Hmgcs2*$^{fl/fl}$ *VillinER/Cre*$^{-/-}$) and *Hmgcs2*$^{\Delta IEC}$ (*Hmgcs2*$^{fl/fl}$ *VillinER/Cre*$^{+/-}$) mice (Figure S2A). Following tamoxifen administration, HMGCS2 was undetectable in colonic IECs by western blot, with no change in the liver (Figures S2B and S2C). βHB was significantly decreased in colonic IECs from *Hmgcs2*$^{\Delta IEC}$ mice (Figure S2D). In contrast, serum βHB was unaffected (Figure S2E), suggesting that the direct impact of intestinal ketogenesis is restricted to the GI tract.

HMGCS2 in IECs was required for KD-mediated protection during EAE. We treated 7- to 9-week-old CONV-R male *Hmgcs2*$^{\Delta IEC}$ and *Hmgcs2*^{WT} mice with tamoxifen daily for 5 days, allowed for a 5-day washout, then put the mice on a KD for 3 days followed by EAE induction (Figure S3A). *Hmgcs2*$^{\Delta IEC}$ mice had significantly increased disease scores over time relative to their *Hmgcs2*^{WT} counterparts (Figure 3A). Disease incidence (Figure 3B) and maximum disease scores were lower in *Hmgcs2*^{WT} mice (Figures 3C and 3D). Circulating βHB levels were not altered between the *Hmgcs2*^{WT} and *Hmgcs2*$^{\Delta IEC}$ mice (Figure 3E). These phenotypic differences were consistent with the significantly higher IL-17a^{+} IFNγ^{+} Th17 cells and IL-17a mean fluorescence intensity within the brains of *Hmgcs2*$^{\Delta IEC}$ mice relative to controls (Figures 3F–3H and S3B).

Finally, we used KE pharmacological administration to rescue disease caused by the genetic deletion of *Hmgcs2* in IECs. We fed 14- to 17-week-old CONV-R male *Hmgcs2*$^{\Delta IEC}$ and

Hmgcs2^{WT} mice a KD or the same KD supplemented with the KE (100 g/kg, Table S1). After 3 days, we induced EAE and tracked disease. Supplementation of the KE significantly increased circulating βHB levels in both *Hmgcs2*$^{\Delta IEC}$ and *Hmgcs2*^{WT} mice compared to unsupplemented KD (Figure S3C). As expected, *Hmgcs2*^{WT} mice were unaffected by the addition of the KE (Figures 3I–3L). In contrast, the KE significantly decreased disease scores over time in *Hmgcs2*$^{\Delta IEC}$ mice (Figure 3I) as well as the incidence rate (Figure 3J). Maximum disease scores of diseased mice were also lower in the KE-supplemented *Hmgcs2*$^{\Delta IEC}$ mice relative to KD controls (Figure 3K), where no KD-KE-fed *Hmgcs2*$^{\Delta IEC}$ mice developed clinical disease by day 30 (Figure 3L). These experiments support the key role of the intestinal production of βHB for the protective effect of a KD during EAE.

The antibiotic ampicillin phenocopies the effects of the ketone ester

Given βHB's potential to alter host[12,40] and microbial[16] cells in the GI tract, we tested whether KE effects are microbiota dependent. Previous work showed that ampicillin rescues EAE in mice on a standard chow diet,[24] but its effects in the context of HFD or KD were unknown. We fed 9-week-old CONV-R female C57BL/6J mice an HFD or HFD-KE for 3 days, then administered ampicillin via their drinking water for 7 days before inducing EAE and tracking disease (Figure S4A). As in previous experiments (Figures 2C–2F), HFD-KE mice had significantly lower disease scores than HFD mice without ampicillin (Figure S4B). Ampicillin reduced EAE scores in HFD mice and showed a trend toward lower disease incidence (Figure S4C), but HFD-KE mice treated with or without ampicillin had similar outcomes. Maximum disease scores were similar across groups, with a slight reduction in ampicillin-treated HFD mice (Figures S4D and S4E). These results suggest that the protective effect of βHB depends on the microbiota, highlighting the need to further explore the impact of diet and KE on gut microbial structure.

Ketogenesis alters the gut microbiota of diseased mice

We hypothesized that intestinal βHB protects from EAE in part by altering the immunomodulatory potential of the gut microbiota. However, it was unclear how a KD and KE would affect the microbiota in diseased mice, as previous studies were in healthy mice.[16] Using 16S rRNA gene sequencing (16S-seq), we profiled the gut microbiota of EAE mice fed HFD, HFD-KE, or KD at 7 days post immunization (mice from Figures 2B–2F). 16S-seq revealed significant shifts in the gut microbiota between diets during EAE (Figure S5). Shannon diversity was higher in HFD-KE and KD groups compared to HFD-fed mice (Figure S5A). Principal coordinate analysis and PERMANOVA testing showed significant differences between HFD-KE and HFD, and between KD and HFD (Figure S5B). KE and KD caused similar changes in the abundance of amplicon sequence variants (ASVs), with some notable exceptions (Figures S5C and S5D). Thus, both diet and βHB supplementation significantly impact the gut microbiota of diseased mice.

The βHB-associated gut microbiota protects from disease

Having shown that βHB impacts the gut microbiota, we next tested the impact of fecal microbiota transplantation (FMT) on EAE phenotypes. We fed 6- to 8-week-old female CONV-R C57BL/6J mice an HFD or HFD-KE for 3 days prior to receiving a commonly used antibiotic cocktail (AVNM: ampicillin, vancomycin, neomycin, and metronidazole) for

1 week to deplete the baseline microbiota.[41,42] FMT was performed daily by oral gavage for 7 days prior to and after EAE induction from 6- to 8-week-old CONV-R female donor mice fed an HFD or HFD-KE for 1–3 weeks (two donors, four recipients per donor, two cages per group; Figure 4A).

FMT from HFD-KE donors significantly reduced EAE severity compared to HFD donors, regardless of the diet of the recipient mice. Recipients of HFD-KE FMT had lower disease scores and incidence rates than those receiving HFD FMT (Figures 4B and 4C). However, maximum disease scores (Figure 4D) and score distributions (Figure 4E) were similar between groups. 16S-seq analysis of the recipient mice revealed that the donor gut microbiota had a significant impact on the gut microbiota that overwhelmed the baseline differences by recipient diet (Figures 4F–4I). This effect was likely due to the repeated oral gavage over 2 weeks. The protective impact of KE was less pronounced than in previous experiments (Figure 2), possibly due to antibiotic pretreatment or variability in disease severity between experiments.[20,30]

Next, we performed a similar FMT experiment using our transgenic mice deficient in intestinal βHB production. Donor $Hmgcs2^{WT}$ and $Hmgcs2^{\Delta IEC}$ mice (two donors per group) were fed a KD for 3 days prior to FMT. Recipient mice of both genotypes were given AVNM via drinking water for 7 days prior to daily gavage for 1 week prior to and following EAE induction (Figure 4J). Disease was tracked for 22 days. Consistent with our KE FMT experiment (Figures 4B–4E), we found that FMT from an $Hmgcs2^{\Delta IEC}$ donor led to significantly higher disease scores irrespective of the genotype of the recipient mice (Figure 4K). Disease incidence was similar in most groups with the exception of a trending lower incidence in the $Hmgcs2^{WT}$ FMT to $Hmgcs2^{WT}$ recipient (Figure 4L). Maximum disease scores of mice that developed disease were lower in mice that received $Hmgcs2^{WT}$ FMT compared to $Hmgcs2^{\Delta IEC}$ FMT, with 38% and 47% of the $Hmgcs2^{\Delta IEC}$ recipients developing maximum disease (Figures 4M and 4N).

Unlike the diet FMT experiment, some effects of host genotype persisted despite having distinct FMT donors. $Hmgcs2^{WT}$ FMT into $Hmgcs2^{WT}$ recipients led to significantly lower disease scores over time compared to $Hmgcs2^{WT}$ FMT into $Hmgcs2^{\Delta IEC}$ mice (Figure 4K). However, irrespective of the recipient genotype, $Hmgcs2^{\Delta IEC}$ FMT resulted in worsened disease over time (Figure 4K). The combined results across both FMT paradigms suggest that intestinal βHB alters the gut microbiota in a manner that ameliorates the EAE model.

Identification of immunomodulatory bacteria linked to diet

Our prior work demonstrated a reproducible decrease in bifidobacterial abundance in both humans and mice fed a KD, resulting in decreased intestinal Th17 activation.[16] However, only a single ASV within the *Bifidobacterium* genus was detected in our initial experiment (Figure S5), which was not significantly altered in response to diet. Furthermore, a pilot experiment in which we orally gavaged *Bifidobacterium adolescentis* strain BD1 to CONV-R mice fed a KD did not significantly impact the EAE phenotype, prompting us to design an unbiased approach to screen for bacteria of interest that could mediate the protective effect of a KD.

Given that previous studies have implicated a range of microorganisms capable of impacting EAE,[43] we aimed to take a reductionist approach to narrow in on members of the microbiota contributing to the protective effect of a KD and KE supplementation. We utilized a method for generating stable *in vitro* communities (SICs) that was initially established using the human gut microbiota.[27] Stool samples from a representative mouse fed the HFD, HFD-KE, or KD collected 7 days post immunization were passaged three times in rich bacterial medium (n = 4–5 SICs/donor; Figure S6A). 16S-seq was used to assess the microbial communities remaining in each SIC. Multiple differences between donor samples persisted despite three rounds of passaging *in vitro*. The KD SICs had significantly lower Shannon diversity than HFD SICs (Figure S6B). Despite a marked divergence from the donor samples (Figure S6C), the SICs from the KD and KE donors were both significantly different from the HFD SICs (Figures S6C and S6D). Overall richness was quite low after passaging, with just 16 unique ASVs detected in the SICs at the endpoint (4–10 ASVs/SIC; Figures 5A and S6E; Table S2) compared to 41, 109, and 128 ASVs in the donor HFD, HFD-KE, and KD samples, respectively. Three ASVs were both abundant and common across all 13 SICs, including *Enterococcus* (ASV4), *Bacteroides* (ASV2), and *Parasutterella* (ASV9). The remaining ASVs were variable between samples and diet groups.

Th17 cells play an important role in the pathogenesis of both human MS and the EAE model.[44–47] Thus, we used a Th17 skewing assay[48,49] to assess the immunomodulatory potential of each SIC. In brief, splenic $CD4^+$ T cells were isolated and skewed to Th17 fate in the presence of cell-free supernatants from our SICs. After 4 days, cells were restimulated before supernatants were collected for IL-17a quantification via ELISA. All of the HFD-derived SICs induced IL-17a, whereas none of the KD-derived SICs had an effect in this assay (Figure 5A); the HFD-KE SICs were mixed, with four out of five inducing IL-17a. Three ASVs were significantly associated with IL-17a levels (Figure 5A), including two negatively associated ASVs annotated as *Lactobacillus* (ASV3 and ASV24; Figures 5B and 5C) and the positively associated *Parasutterella* (ASV9; Figure S6F). *Lactobacillus* was recently renamed *Ligilactobacillus*; however, we opted to refer to it as *Lactobacillus* for consistency with previous studies.[50–52]

A *Lactobacillus* isolate and metabolite protect from disease

We sought to isolate a representative *Lactobacillus* strain from our SICs to enable more controlled experiments. We anaerobically plated a KD-SIC (Figure 5A) on *Lactobacillus*-selective medium (MRS). Identification by matrix-assisted laser desorption/ionization mass spectrometry revealed two colonies that matched the *L. murinus/animalis* fingerprint; a representative isolate was validated by full-length 16S-seq (Table S3). Multiple lines of evidence suggested that this isolate matched ASV24 from the SICs: (1) ASV24 was the only ASV assigned to *Lactobacillus* in the source SIC (KD-SIC replicate 4); and (2) the 16S rRNA gene sequence was 100% identical, with 100% coverage (NCBI BLASTN), to the representative sequence from ASV24 (Table S3). We designated this isolate *L. murinus* KD6.

Lactobacilli, including *L. murinus*, convert tryptophan (Trp) to indole-3-lactate (ILA), which inhibits Th17 cell production of IL-17a.[51,53] To assess whether *L. murinus*

KD6 had genes involved in ILA production, we generated a finished genome using a hybrid of short- and long-read sequencing. Trp is deaminated via aromatic amino acid aminotransferases (ArATs) to form indole-3-pyruvate (IPYA) which is then dehydroxylated by phenyllactate dehydrogenases (FldH) or D-lactate dehydrogenases (D-LDH) to make ILA[50,52–54] (Figure 6A). We identified four genes homologous to aminotransferases in the *L. murinus* KD6 genome. This includes a putative aspartate aminotransferase (AspAT) with significant homology to an annotated AspAT from known ILA-producing species, including *Clostridium sporogenes, Lactobacillus reuteri*, and *L. murinus* (Figure 6B; Tables S4 and S5). We also detected four putative *LDH* genes in the *L. murinus* KD6 genome, including a candidate D-lactate dehydrogenase (*D-LDH*) with significant homology to genes found in ILA producers (Figure 6B; Tables S4 and S5). We then used targeted liquid chromatography-mass spectrometry to confirm the production of ILA from *L. murinus* KD6 and the positive control strain *L. reuteri* ATCC23272[50] (Figure 6C). As expected,[51,53] ILA inhibited the production of IL-17a by Th17 cells in our skewing assay (Figure 6D).

We next tested the impact of *L. murinus* KD6 and ILA on EAE. HFD-fed mice were orally gavaged with a vehicle, *L. murinus* (10^8 CFU), or ILA (20 mg/kg) every other day for the duration of the experiment. EAE was induced 4 days after the first gavage, and disease was tracked. Disease scores over time were significantly lower in response to both *L. murinus* and ILA relative to vehicle controls (Figure 6E). Disease incidence was highest in the HFD group (Figure 6F). The probability of survival in the HFD group (28% by day 18) was significantly lower than in the *L. murinus* (74%) and ILA (68%) treated groups (Figure 6G). 72% of the HFD controls reached a disease score >4.5, whereas the other two groups were mixed (Figures 6H and 6I). These data suggest that *L. murinus* protects mice during EAE due to the production of the anti-inflammatory metabolite ILA.

We next wanted to assess whether ILA-producing microbes and/or ILA are changed in response to a KD and/or βHB-KE supplementation. We leveraged our previous 16S-seq dataset from mice fed an HFD, HFD-KE, or KD (Figure S5). While there was no difference in ASV23 *L. murinus* abundance between groups, there was a significant increase in the abundance of ASV24 *L. reuteri*, another known ILA producer,[55] in both HFD-KE and KD groups compared to HFD (Figure 6J). The abundance of ASV24 *L. reuteri* was also significantly higher in mice with mild or no disease symptoms compared to mice with more severe disease (score of >2.5) (Figure 6K). Additionally, we quantified fecal levels of ILA in SJL/J mice on an HFD, HFD-KE, or KD (from Figures 2G–2J) at days 7, 21, and 28 post EAE induction. At days 7 and 28, mice on HFD-KE had significantly higher fecal ILA than HFD-fed mice, while KD mice showed no difference at any time point (Figures S7A–S7C). These data suggest that KD and βHB-KE enrich for known ILA producers and that βHB-KE supplementation is sufficient to elevate fecal ILA level during disease.

Lactobacilli are not the only source of ILA within the gut microbiota. ILA production has been observed in diverse bacterial species spanning multiple phyla.[56] We investigated the impact of βHB on the levels of ILA-producing microbes by reanalyzing published data for human *ex vivo* stool communities cultured with or without βHB for 24 h.[16] We defined ILA-producing microbes as microbes with fold change of ≥4 over controls by mass spectrometry.[56] The relative abundance of ILA-producing microbes was significantly

increased in response to βHB (Figures S7D and S7E). We hypothesized that βHB increased the abundance of ILA-producing microbes by selective growth promotion. Supporting this hypothesis, treatment with 12.5 mM βHB resulted in improved growth of *L. murinus* compared to control bacteria, *B. adolescentis* BD1, as measured by shifted growth curves (Figures S7F and S7G) and decreased time to reach mid-exponential growth in monocultures grown in brain heart infusion (BHI) medium (Figure S7H). At higher concentrations, 50 mM βHB inhibited growth of both *L. murinus* and *B. adolescentis* (Figures S7F and S7G); however, *L. murinus* growth was less inhibited than that of *B. adolescentis* as measured by an increased carrying capacity and increased growth rate compared to no treatment (Figures S7I and S7J). Together, these data suggest that βHB directly shapes the microbiota composition to favor ILA-producing microbes by having a stronger growth-inhibitory impact on non-ILA-producing members of the microbiota communities. These data provide a potential mechanism for how a diet-responsive host metabolite βHB shapes the microbial community structure.

Notably, multiple studies support the clinical relevance of ILA whereby ILA is one of the most depleted serum metabolites in MS compared to controls,[57,58] and MS patients have a decreased abundance of ILA-producing gut bacteria.[58] We wanted to investigate these findings in an independent cohort of MS subjects (iMSMS) using our metric for ILA-producing microbes. ILA-producing microbes were significantly decreased in MS subjects compared to healthy controls, driven by the untreated MS patients; treated subjects had levels of ILA-producing bacteria similar to those of controls (Figure 6L). ILA-producing bacteria were inversely associated with disease severity (Figure 6M). Taken together, these findings support the clinical relevance of our results.

DISCUSSION

We provide evidence that a microbiome-dependent pathway mediates the protective effects of a common dietary intervention against a neuroinflammatory disease. Building on previous human[6–8] and mouse[9–11] studies, we confirmed that a KD mitigates disease in the EAE mouse model. Our findings highlight the importance of considering individual variations in gut microbiota in future research to better understand the differing responses to KD seen in MS patients[6–8] and mouse[9–11] studies.

Surprisingly, we discovered that oral delivery of a βHB-KE can mimic the protective effects of a KD. If this finding holds in humans, βHB supplementation alone could offer a viable therapeutic alternative to the full KD. The translational implications are profound, as KDs are difficult to maintain and can have negative side effects.[59] Our identification of βHB as a key player provides a way to circumvent these barriers and provides a more general proof of concept for the ability to distill the activity of a complex diet down to a single bioactive molecule.

Our data from transgenic mice lacking intestinal *Hmgcs2* expression highlight the need to study tissue-specific production of βHB and other diet-dependent metabolites. Surprisingly, local GI βHB production was essential for the full neuroprotective effect of a KD, even without changes in circulating βHB levels. While other tissues such as the liver may also

contribute to βHB levels, these findings suggest that GI βHB levels are more indicative of the effective KE dose. Previously, we found that GI βHB tissue levels rose similarly with KE supplementation and KD, while serum and gut lumen levels were higher with KD.[16] These results enhance the understanding of gut-neuroinflammation interactions, showing how a host metabolite can signal the brain via a microbial effector.

We identified that a *Lactobacillus* isolate, *L. murinus* KD6, and the *Lactobacillus*-produced metabolite ILA are each sufficient to rescue disease. Prior studies showed that supplementation with *L. murinus* reduced EAE disease severity in mice on a high-salt diet and that ILA inhibits Th17 cells *in vitro*.[51] Our data extend this work by showing that: (1) ILA protects against EAE; (2) βHB-KE treatment elevates fecal ILA levels; and (3) ILA contributes to the protective effects of βHB. As the genes for bacterial ILA production are known,[50,52–54] follow-up studies of isogenic *L. murinus* or other bacterial strains varying in ILA production would help dissect the host response in EAE. These engineered bacteria could even enable more controlled MS patient trials, given the potential broad impacts of probiotics for MS.

There are several potential ways the gut microbiota can influence MS. While segmented filamentous bacteria (SFB or *Candidatus arthromitus*) and an *Allobaculum* isolate worsen EAE by activating Th17 cells,[22,24] *Bacteroides fragilis* offers protection by increasing $Foxp3^+$ regulatory T cells.[60] Inspection of our 16S-seq data did not reveal these EAE-associated species, suggesting they do not influence our results. Future studies in gnotobiotic mice are needed to explore how these and other immunomodulatory gut bacterial species interact under different diets.

Our study integrates and extends multiple prior observations. This includes data linking a ketogenic diet to protection from MS,[6–11] the KD to shifts in the gut microbiota,[16,17] the production of ILA by *Lactobacillus*,[51,53] the suppression of Th17 cells by ILA,[51] and the key role for Th17 cells in MS pathogenesis.[44–47] Thus, it is critical to consider both host and microbial metabolism, including key bioactive compounds such as βHB and ILA. Our findings add to the growing literature on other diets that elevate βHB, including intermittent fasting and caloric restoration, which have shown some efficacy in MS patients and mouse models.[9,61–64] Targeting bioactive compounds such as βHB and ILA could help surmount potential issues of a lack of long-lasting effects of dietary intervention in MS subjects.[65] The pathway we have identified herein provides a common mechanism through which these diverse dietary interventions may impact MS. More broadly, our results set the stage to perform similar studies in other autoimmune diseases and for alternative dietary interventions, providing new insights into the complex mechanisms that link diet, the gut microbiome, and host immunity.

Limitations of the study

There are several limitations to our study deserving of follow-on work. While βHB inhibits microbiota growth,[16] the mechanism and implications are unknown. We focused on the gut microbiome, but the dietary benefits for MS likely involve βHB's direct effects on the host,[32] such as inflammasome inhibition.[33,34] The inflammasome shapes the microbiota's immunomodulatory potential,[66–68] offering another way βHB might affect host-microbiome

interactions. Importantly, βHB can cross the blood-brain barrier and have immune effects in the central nervous system.[69] Tryptophan metabolites, including ILA, influence Th17 responses through the aryl hydrocarbon receptor (AHR).[70–72] Therefore, it will be important in future studies to investigate the role of host factors including the inflammasome and/or AHR in the mediation of the protective effect of a KD and KE supplementation.

Investigating other immunomodulatory effects of KD- or KE-altered microbiota could reveal additional insights, as Th17 cells are not the sole contributors to MS and EAE. It is also essential to examine other Th17-skewing models, such as IL-23 and IL-1β, implicated in EAE pathogenesis.[73] Additionally, diet-induced changes in immune function could impact the gut microbiota. Future studies in humans and mouse models with varied diets and therapies will be important for exploring the translational relevance of ketone bodies, lactobacilli, and ILA. While βHB-KE raises fecal ILA during disease, no change was observed with a complex KD, possibly due to differences in timing, metabolism, or other factors that remain to be explored.

RESOURCE AVAILABILITY

Lead contact

Further information and requests for resources and reagents should be directed to and will be fulfilled by the lead contact, Peter Turnbaugh (peter.turnbaugh@ucsf.edu).

Materials availability

This study does not contain newly generated materials.

Data and code availability

- All data are available in the main text, the supplemental tables, datasets, or deposited as listed below. This paper does not report original code. Any additional information required to reanalyze the data reported in this paper is available from the lead contact upon request.
- 16S-seq and *L. murinus* whole-genome sequence are deposited under NCBI Bioproject: PRJNA1032118.

STAR★METHODS

EXPERIMENTAL MODEL AND STUDY PARTICIPANT DETAILS

Mice—All animal experiments were conducted under protocols (AN200526 and AN199820) approved by the UCSF Institutional Animal Care and Use Committee with the exception of the experiment in Figure S1E, which was performed at the University of Wisconsin - Madison under the IACUC protocol M006785. Germ-free C57BL/6J mice were born at UCSF and CONV-R SPF C57BL6/J mice were purchased from Jackson Laboratory. Germ-free mice were maintained within the UCSF Gnotobiotic Core Facility. Mice age ranged from 8 to 16-week-old and mice were assigned to groups to achieve similar age distribution between groups. Mice were housed at temperatures ranging from 67 to 74°F

and humidity ranging from 30 to 70% light/dark cycle 12h/12h. No mice were involved in previous procedures before experiments were performed.

Hmgcs2^{WT} (*Hmgcs2*$^{fl/fl}$ *VillinER/Cre*−/−) or *Hmgcs2*$^{\Delta IEC}$ (*Hmgcs2*$^{fl/fl}$ *VillinER/Cre*$^{+/-}$) mice on C57BL6/NJ substrain hybrid background were generated. *Hmgcs2*$^{fl/fl}$ mice were generated in collaboration with the inGenious Targeting Laboratory (Ronkonkoma, NY). Briefly, BF1 clone C57BL/6N mouse embryonic stem (ES) cells harboring an expression construct for FLP recombinase were electroporated with a donor vector targeting exon 2 of the *Hmgcs2* locus (NM_008256), along with Cas9 and synthetic guide RNAs. Targeting exon 2 results in a frameshift mutation and resulting nonsense (premature stop) encoding *Hmgcs2* transcript. After selection for neomycin resistance using G418, and confirmation of successful targeting using both Southern blots and PCR, targeted ES cells were microinjected into Balb/c blastocysts, and chimeras with a high percentage black coat color were mated to C57BL/6N WT mice to generate Germline *Neo* Deleted mice (*Hmgcs2*$^{fl/+}$). PCR and DNA sequencing were used to confirm (*i*) successful flanking of exon 2 with *loxP* sites, (ii) the loss of the neomycin resistance-encoding gene, and (*iii*) the absence of an FLP recombinase transgene in the progeny. Transgenic mice harboring a tamoxifen-inducible Cre recombinase under the control of the villin-promoter (VillinER/Cre, C57BL/6J)[85] were a gift from M. Kattah (UCSF). *Hmgcs2* was specifically and inducibly deleted from intestinal epithelial cells (IECs). These mice were made by crossing *Hmgcs2*$^{fl/fl}$ mice (shipped from the University of Minnesota) with *VillinER/Cre*$^{+/-}$ and then breeding mice to homozygosity. For experimental mice, *Hmgcs2*$^{fl/fl}$ *VillinER/Cre*$^{-/-}$ mice were bred with *Hmgcs2*$^{fl/fl}$ *VillinER/Cre*$^{+/-}$ mice to produce *Hmgcs2*^{WT} - *Hmgcs2*$^{fl/fl}$ *VillinER/Cre*$^{-/-}$ and male mice with *Hmgcs2* specifically deleted from intestinal epithelial cells *Hmgcs2*$^{\Delta IEC}$ - *Hmgcs2*$^{fl/fl}$ *VillinER/Cre*$^{+/-}$. *Hmgcs2*^{WT} and *Hmgcs2*$^{\Delta IEC}$ mice were reared at UCSF.

Hmgcs2^{WT} or *Hmgcs2*$^{\Delta IEC}$ were induced with 5 daily i.p. injections of 100 μL of tamoxifen at a concentration of 10 mg/mL. Tamoxifen was prepared by dissolving 100 mg/mL of tamoxifen in 100% ethanol, incubating for 30 min at 56°C, vortexing, then diluting 1:10 in corn oil to a final concentration of 10 mg/mL. After tamoxifen injections, mice had a 5 day washout period before starting on their specific diets. Genotype of mice was confirmed with PCR where DNA was extracted from mouse tissue using Direct PCR (Thermo Fisher) according to the manufacturer's instructions. Briefly, 150 μL of Direct PCR and 3 μL Proteinase K was added to the tissue then incubated in 56°C water bath overnight. 100 μL of the sample was then transferred to PCR strip tubes and incubated for 1 h at 85°C. For PCR, 1 μL extracted DNA, 12.5 μL AmpliTaq Gold master mix (Thermo Fisher), 1 μL forward primer (1 μM final concentration), 1 μL reverse primer (1 μM final concentration) and 9.5 μL water was combined with the following primer sequences to detect Cre presence: Cre forward - 5′ TTC CCG CAG AAC CTG AAG ATG 3′; Cre reverse: - 5′ CCC CAG AAA TGC CAG ATT ACG 3′. *Hmgcs2*$^{fl/fl}$ was homozygous and confirmed initially with the following primers: HMGCS2 forward - GTG AGT TCT GTG CCT GAC TG; HMGCS2 reverse - CAG AGC TGC AAG ATG AGT AAC TG. The following PCR cycle conditions were used for Cre detection (1. 95°C for 10 min; 2. 95°C for 30 s; 3. 60°C for 30 s; 4. 72°C for 30 s; 5. repeat steps 2–4 34x; 6. 72°C for 5 min; 7. 11°C hold) and for *Hmgcs2* detection (1. 95.0°C 10 min; 2. 95.0°C 5 s; 3. 55.0°C 30 s; 4. 72.0°C 10 s; 5. Repeat steps 2–4, 29x; 6. 72.0°C 5 min; 7. 4.0°C hold). Only male mice were used for *Hmgcs2* experiments as in

our initial experiments female mice on a KD did not develop clinical symptoms of disease in either *Hmgcs2*^{WT} or *Hmgcs2*$^{\Delta IEC}$ mice. For non-transgenic mouse experiments both male and female mice were used for initial experiments and then female mice were used for later experiments to control for the potentially sexually dimorphic presentation of EAE.[86]

Diets—All diets were provided *ad libitum*. Semi-purified diets were purchased from Envigo, and the ingredients used in these diets are listed in Table S1. Before experimental diets started, mice were fed standard chow diet (Lab Diet 5058) in the SPF facility, while standard autoclaved chow diet (Lab Diet 5021) was used in the gnotobiotic facility. For Figure S1E performed at UW-Madison, mice were fed a Teklad 2019 diet before starting on HFD or KD. All diets used for gnotobiotic experiments were either autoclaved or irradiated to ensure sterility. For the design of the diets supplemented with KE: 10% C6X2-βHB KE was added at the expense of fat. C6X2-βHB is estimated to contain 8 kcal/g and is composed of fatty acids ester-linked to the ketone body β-hydroxybutyrate.

Antibiotic water treatments—Where specified mice were treated *ad libitum* with antibiotic water including 0.1 g/L ampicillin or a 4 antibiotic cocktail AVNM (1 g/L ampicillin, 0.5 g/L vancomycin, 1 g/L neomycin, 1 g/L metronidazole). Antibiotic water was prepared from autoclaved tap water with 0.2 μm filtering after the antibiotic(s) were added.

Experimental autoimmune encephalomyelitis (EAE) in C57BL/6J mice—EAE was induced with slight modification of previous descriptions.[30] An emulsion of a 100 mg/100 μL of $pMOG_{35–55}$ (Tocris; cat# 25681) resuspended in sterile 1X phosphate buffered saline (PBS) and complete Freund's adjuvant (CFA - 4 mg/mL: heat killed Mycobacterium tuberculosis (MTB) Fisher Scientific; cat# DF3114338 at 4 mg/mL in incomplete Freund's adjuvant Millipore Sigma; cat# F5506) was prepared by passing through a three-way stopcock connected pair of 10 mL syringes for 5 min or until emulsion was stable by the water drop test. 100 μL of the MOG and CFA emulsion was injected into mice via subcutaneous injection. Directly following MOG injections, 500 ng of pertussis toxin (PTX) (Millipore Sigma; cat# P2708) in 100 μL of PBS was injected via i.p. injections. 500 ng PTX in 100 μL of PBS was again injected via i.p. the day following immunization. Mice were weighed and scored for disease daily for the duration of the experiment. EAE disease courses were tracked for 16–30 days for a combination of logistical and scientific rationales. To assess immune responses at peak disease some EAE experiments were tracked for shorter time periods.

EAE scoring was outlined as follows: 0 = no obvious signs of disease; 0.5 = partial tail weakness; 1 = limp tail; 2 = limp tail and hindlimb weakness; 2.5 = limp tail and impairment in righting reflex; 3 = one hindlimb paralyzed; 3.5 = bilateral hindlimb paralysis; 4 = bilateral hindlimb paralysis and forelimb paresis; 4.5 = limp tail, complete hind leg and partial front leg paralysis, mouse is minimally moving around the cage but appears alert and feeding. Euthanasia required after the mouse scores 4.5 for 24 h; 5 = moribund: complete hind and partial front leg paralysis, no movement around the cage, mouse is not alert, has minimal movement in the front legs, or barely responds to contact; euthanasia as soon as possible.

Experimental autoimmune encephalomyelitis (EAE) in SJL/J mice—EAE was induced with slight modification of previous descriptions.[37,38] 9-week-old female SJL/J mice from Jackson Labs were fed HFD, HFD-KE, or KD for 5 days prior to EAE induction. Mice that developed tail lesions (1 animal, in our case) were immediately euthanized and removed from the experiment given SJL/J mice with tail lesions do not develop EAE.[38] To induce EAE, an emulsion of a 100 μg/100 μL of $PLP_{139–151}$ (Genscript; custom synthesis with >95% purity by HPLC and <10EU/mg endotoxin, sequence: HSLGKWLGHPDKF [unmodified]) resuspended in sterile 1X PBS and CFA (4 mg/mL: heat killed Mycobacterium tuberculosis (MTB) Fisher Scientific; cat# DF3114338 at 4 mg/mL in incomplete Freund's adjuvant Millipore Sigma; cat# F5506) was prepared by passing through a three-way stopcock connected pair of 10 mL syringes until emulsion was stable by the water drop test. 100 μL of the PLP and CFA emulsion was injected into mice via subcutaneous injection. Directly following PLP injections, 200 ng of pertussis toxin (PTX) (Millipore Sigma; cat# P2708) in 50 μL of PBS was injected via i.p. injections. 200 ng PTX in 50 μL of PBS was again injected via i.p. the day following immunization.

Mice were weighed and scored for disease every day for the duration of the experiment. Mice that became singly housed due to death of cagemates were provided additional enrichment. SJL/J EAE was scored in accordance with the Hooke EAE rubric and modified Hooke rubric for recovery.[87]

Fecal microbiota transplants—Fecal donor mice were put on their respective diets for 1–3 weeks prior to fecal collection with 2 donor mice cohoused per group. Donor fecal samples were collected from mice the day preceding transplantation and then frozen at −80°C before the next day, being resuspended in 1:10 g/mL sterile pre-equilibrated PBS in an anaerobic Coy chamber. Each sample was vortexed for 1 min and left to settle for 2 min, and the supernatants were then used for gavage. 100 μL of each sample was administered by oral gavage into the mice. Recipient mice were put on respective diets 3 days before receiving the AVNM cocktail of antibiotics in drinking water for 7 days (prepared as described above). AVNM water was then removed and daily gavage of FMT material began 7 days preceding EAE induction, then continued for 7 days post EAE induction.

L. murinus* engraftment—L. murinus* KD6 was incubated aerobically at 37°C overnight in 10 mL MRS media (Difco Lactobacilli MRS agar, BD Biosciences, cat# 288210). Cultures were centrifuged 10 min at 2500 rpm, washed with sterile 1X PBS, centrifuged 10 min at 2,500 rpm, and then resuspended in sterile 1X PBS for oral gavage. Mice were gavaged with 200 μL of *L. murinus* KD6 (10^8 CFU) every other day for the duration of the experiment.

Indole-3-lactate (ILA) treatment—A solution of ILA (DL-Indole-3-lactic acid; Sigma; cat# I5508) in sterile 1X PBS was made by vortexing before and after a 10 min incubation at 56°C to fully dissolve ILA. Mice received a dose of 20 mg/kg ILA every other day via oral gavage as described previously.[88,89] Control HFD mice received oral gavages of 200 μL sterile 1X PBS (vehicle) every other day.

METHOD DETAILS

Brain leukocyte isolation—Brain leukocytes were isolated with slight modifications of previously described techniques.[90] Brains were dissected out of the mice and put into 4 mL ice-cold 1X PBS in 6 well plates on ice. Then, brains were cut into small pieces with scissors until small enough to pass through an 18 gauge needle several times in PBS to homogenize tissue. This tissue homogenate was then passed through a 70 μm filter and filters were then washed with 10 mL ice-cold 1X PBS. Filtered homogenate was centrifuged at 2,000 rpm for 10 min and the supernatant was removed. Cells were resuspended in 5 mL of 30% Percoll (VWR; cat# 89428-524) and then overlaid on top of 5 mL 70% Percoll at room temperature. Percoll gradients were then centrifuged at 2,000 rpm at 25°C for 25 min, with no brakes (deceleration set to 0) and lowest acceleration (acceleration set to 1). Cells at the interface were collected, washed with 1X PBS, and prepared for flow cytometry analysis.

Spleen cell isolation—Spleen cells were prepped through gentle mashing with a syringe plunger then filtered through a 40 μm filter. Cells were pelleted by centrifugation (2,000 rpm 5 min) and then treated with 1 mL 1X red blood cell (RBC) Lysis Buffer (Biolegend; cat# NC9067514) to lyse red blood cells. Cells were pelleted again (2,000 rpm, 5 min) and then washed in 1X PBS.

Flow cytometry—Immune cells were isolated from the brain and spleen as described above. Surface staining for lymphocytes was done in staining buffer (1X Hank's Balanced Salt Solution (HBSS), Life Technologies; cat# 14170161) supplemented with 10 mM hydroxyethyl piperazineethanesulfonic acid (HEPES, Fisher Scientific; cat# NC0734307), 2 mM ethylenediaminetetraacetic acid (EDTA, Fisher Scientific; cat# AM9260G), and 0.5% (v/v) heat inactivated fetal bovine serum (Life Technologies; cat# 10438026) for 20 min at 4°C. Cells were then washed twice in supplemented 1X HBSS and analyzed via flow cytometry. The following antibodies were used: anti-CD3 (Clone: 17A2, Fluorophore: FITC, Fisher Scientific; cat# 501129303), anti-TCRβ (Clone: H57-597, Fluorophore: PE-CF594, Fisher Scientific; cat# BDB562841), anti-CD4 (Clone: GK1.5, Fluorophore: BV786, Fisher Scientific; cat# BDB563331), and live/dead staining was performed using aqua LIVE/DEAD Fixable Dead Cell Stain Kit (Fisher Scientific; cat# 501121526). Cells were stimulated with a cell stimulation cocktail (Fisher Scientific; cat# 501129036) containing PMA and ionomycin according to the manufacturer's instructions and Golgi Plug (1 μL/ sample) (Fisher Scientific; cat# BDB555029) for 4–6 h at 37°C. Cells were surface stained, washed, and then fixed/permeabilized in 100 μL fixation and permeabilization buffer (Fisher Scientific; cat# BDB555028). Cells were washed twice in permeabilization/wash buffer (Fisher Scientific; cat# BDB555028) and then stained for intracellular cytokines with the following antibodies: anti-IFNγ (Clone: XMG1.2; Fluorophore: BV421; Fisher Scientific; cat# BDB563376) and anti-IL17a (Clone: ebio17B7; Fluorophore: PE-Cyanine7; Fisher Scientific; cat# 501129407). Cells were washed twice with permeabilization/wash buffer and then placed in a staining buffer for flow cytometry analysis. Cell population gating was done using isotype and single stain controls. Gating strategies and which figures they correspond to are outlined in Figure S1. The flow cytometry data were collected with a

BD LSR Fortessa and analyzed with FlowJo software (version 10.6.1). All antibodies are included in the key resources table.

Immunoblotting—Flash frozen liver and isolated colonic intestinal epithelial cells (IECs) were lysed in RIPA buffer. IECs were isolated from mouse colons using the following workflow. Colons were splayed longitudinally with mucus removed and cleaned. Colons were then stored in complete RPMI - 10% heat inactivated fetal bovine serum (Life technologies; cat# 10438026), 100 units per mL penicillin and streptomycin (Thermo Fisher; cat# 15070063), glutamax (Gibco; cat# 35050061), sodium pyruvate (Life Technologies; cat# 11360070), HEPES (Fisher Scientific; cat# NC0734307), and nonessential amino acids (Life Technologies; cat# 11140050) on ice. Media was removed by filtering through a 100 μM filter, and remaining tissue incubated in 1X HBSS - without Ca2+ and Mg2+ containing 5 mM EDTA (Fisher Scientific; cat# AM9260G) and 1 mM DL-Dithiothreitol (DTT; VWR; cat# 97063-760) for 45 min at 37°C on a shaker at 200 rpm. Samples were filtered through a 100 μM filter and IECs were collected from the flow-through. Immunoblotting with an Hmgcs2 specific antibody rabbit anti-mHMGCS2 (Santa Cruz Biotechnology Inc.; cat# sc-393256) at a 1:2000 dilution and GAPDH (Prointech; mouse anti-mGAPDH; cat# 60004) at a 1:10,000 dilution was performed. Secondary antibodies conjugated to horseradish peroxidase were goat anti-rabbit IgG (Southern Biotech; cat# 4030-05); 1:50000 for Hmgcs2 and Goat Anti-Mouse IgG (Abcam; cat# Ab6708); 1:2000 for anti-mGAPDH.

β-hydroxybutyrate (βHB) quantitation—For measurements of circulating βHB, blood was obtained from mice immediately following euthanasia. Serum was collected with a serum separator (BD Microtainer cat# 365978), centrifuged at 13,000 rpm for 10 min at 4°C, and frozen at −80°C until use. IECs were isolated as described in the Immunoblotting section. Serum and IECs were extracted as previously described.[91,92] Briefly, samples were extracted with 1 mL (IECs) or 80 μL (serum) of ice-cold methanol [80% v/v], followed by homogenization. After centrifugation, the supernatants were dried in vacuum and reconstituted in 100 μL (IECs) or 50 μL (serum) of methanol (3% v/v). Quantitative analysis was performed with a Dionex UltiMate 3000 quaternary HPLC system connected to Exactive Plus Orbitrap mass spectrometer (Thermo Fisher Scientific, Waltham, MA) with a Waters XSelect HSS T3 column (2.1 mm × 100 mm, 2.5 μm). Data were normalized by a ^{13}C stable isotope labeled internal standard (Cambridge Isotope Laboratories, Inc., Tewksbury, MA). The results were quantified using a standard curve with concentrations ranging from 0.78 μM to 50 μM. For quantification of βHB during EAE experiments (Figures S1A and S1F), βHB was quantified using the Precision Xtra blood glucose and ketone monitoring system (Abbott; cat# 98814-65) using blood β-Ketone test strips (Abbott; cat# ART07249) in *ad libitum* fed mice in the morning (in the 1st 6 h of the 12 h light cycle). Briefly, a drop of tail blood was applied to the β-Ketone test strip inserted in the Precision Xtra blood.

Stable *in vitro* communities (SICs)—SICs were derived from HFD, HFD supplemented with a βHB ketone ester (HFD-KE), or a ketogenic diet (KD) mouse stool sample collected 7 days post EAE induction (1 donor/group, 4–5 independent SICs/donor sample). Incubations were performed anaerobically, as described.[27] Briefly, 100 mg fecal

matter was resuspended in 1 mL brain heart infusion media supplemented with L-cysteine (0.05% w/v), hemin (5 μg/mL), and vitamin K (1 μg/mL) (BHI^{CHV}) with 15% glycerol. Samples were vortexed to suspend the fecal pellets. Sample debris was allowed to settle for 5 min and 500 μL of the supernatant was transferred to a fresh tube. In a 96 well plate, 195 μL of BHI^{CHV} media and 5 μL of each fecal slurry was added to each well. Communities were grown for 48 h at 37°C in an anaerobic chamber (Coy Laboratory Products, 2%–5% H_2, 20% CO_2, balance N_2). Communities were passaged a total of 3 times (initial incubation with 2 additional passages) by adding 5 μL of the previous culture to 195 μL of fresh BHI^{CHV} media and growing an additional 48 h. Cell pellets from the third passage were then used to extract DNA for 16S rRNA gene sequencing. Cell free supernatants (CFS) were collected by centrifuging samples for 10 min at 2,500 rpm and then passing the resulting supernatant through a 0.2 μm filter for use in our Th17 skewing assay.

Bacterial strain isolation, culturing, and identification—To isolate individual strains from our SICs we plated on MRS (Difco Lactobacilli MRS agar, BD Biosciences, cat# 288210) plates at 37°C in an anaerobic chamber (Coy Laboratory Products, 2%–5% H_2, 20% CO_2, balance N_2) for 48 h and selected for individual colonies with streak purification of colonies with distinct morphologies. *L. murinus* KD6 was isolated from a KD-SIC (KD-SIC replicate 4 Figure 5A) on MRS media plates. The L. *murinus* KD6 isolate was identified as *Lactobacillus murinus/animalis* by 16S rRNA gene sequencing amplifying between V1 and V9 with bi-directional sequencing (Azenta Life Sciences) and annotation using NCBI BLASTN with the rRNA_typestrains/16S_ribosomal_RNA database. Species-level annotation to *Lactobacillus murinus* was independently validated using a MALDI Biotyper Sirius (Bruker) according to manufacturer's instructions with direct transfer, extended direct transfer, and extraction sample preparation methods according to manufacturer's instructions. Briefly, for direct transfer for each sample a smear of an isolated colony was applied as a thin film to the MALDI target plate (MBT Biotarget 96 US IVD; cat# 1840380). Then, 1 μL of matrix solution (10 mg/mL of α-cyano-4-hydroxy-cinnamic acid (HCCA) in Bruker's solvent (50% acetonitrile, 47.5% water, 2.5% trifluoroacetic acid) was added on top of smear and dried at room temperature. For extended direct transfer, the same procedure was performed as the direct but with an additional step of adding 1 μL of 70% formic acid and air drying at room temperature before matrix application. For extraction sample preparation, using an inoculation loop, a single colony was transferred to 300 μL of HPLC-grade water and mixed until the material was in suspension. Then 900 μL of 100% ethanol was added and mixed by vortexing. Samples were pelleted with a 2 min 15,000 rpm centrifugation and the supernatant was removed. Samples were pelleted again with a 2 min 15,000 rpm centrifugation and residual ethanol was removed. Samples were then air dried at room temperature for at least 5 min. Then, 25 μL of 70% aqueous formic acid was added and vortexed to resuspend the pellet. 25 μL of 100% acetonitrile was then added and mixed by vortexing. Samples were then centrifuged 2 min 15,000 rpm and 1 μL of the supernatant was applied to the MALDI target plate. A BTS (*Escherichia coli*) was used as a calibration standard.

DNA extraction and whole genome sequencing of L. *murinus* KD6—DNA extraction and whole genome sequencing with Illumina and Nanopore sequencing was performed by Seqcenter (https://www.seqcenter.com/).

DNA extraction: ZymoBIOMICS DNA Miniprep Kit. A cell pellet (10^9 CFU) of *L. murinus* KD6 was resuspended in 750 µL of lysis solution. Cells suspended in lysis solution were transferred into the ZR BashingBeadTM Lysis Tubes and mechanically lysed using the MP FastPrep-24 lysis system with 1 min of lysis at maximum speed and 5 min of rest for 5 cycles. Samples were then centrifuged at 10,000 rcf for 1 min. 400 µL of supernatant was transferred from the ZR BashingBead Lysis Tube to a Zymo-Spin III-F Filter and centrifuged at 8,000 rcf for 1 min. 1,200 µL of ZymoBIOMICS DNA Binding Buffer was added to the effluent and mixed via pipetting. 800 µL of this solution was transferred to a Zymo-Spin IICR Column and centrifuged at 10,000 rcf for 1 min. This step was repeated until all material was loaded onto the Zymo-SpinTM IICR Column. DNA bound to the Zymo-Spin IICR Column was washed 3 times with 400 µL and 700 µL of ZymoBIOMICS DNA Wash Buffer 1 and then 200 µL of ZymoBIOMICS DNA Wash Buffer 2 with a 1-min spin down at 10,000 rcf for each, respectively. Washed DNA was eluted using 75 µL of ZymoBIOMICS DNase/RNase Free Water following a 5-min incubation at room temperature and a 1-min spin down at 10,000 rcf. The Zymo-Spin III-HRC Filter was prepared using 600 µL of the ZymoBIOMICS HRC Prep Solution and a centrifugation at 8,000 rcf for 3 min. Eluted DNA was then purified by running the effluent through the prepared Zymo-SpinTM III-HRC Filter. Final DNA concentrations were determined via Qubit.

Nanopore: Sample libraries were prepared using the PCR-free Oxford Nanopore Technologies (ONT) Ligation Sequencing Kit (SQK-NBD114.24) with the NEBNext Companion Module (E7180L) to manufacturer's specifications. No additional DNA fragmentation or size selection was performed. Nanopore sequencing was performed on an Oxford Nanopore a MinION Mk1B sequencer or a GridION sequencer using R10.4.1 flow cells in one or more multiplexed shared-flow-cell runs. Run design utilized the 400 bps sequencing mode with a minimum read length of 200bp. Adaptive sampling was not enabled. Guppy1 (v6.4.6) was used for super-accurate basecalling (SUP), demultiplexing, and adapter removal. No quality trimming has been performed.

Illumina: Illumina sequencing libraries were prepared using the tagmentation-based and PCR-based Illumina DNA Prep kit and custom IDT 10bp unique dual indices (UDI) with a target insert size of 320 bp. No additional DNA fragmentation or size selection steps were performed. Illumina sequencing was performed on an Illumina NovaSeq 6000 sequencer in one or more multiplexed shared-flow-cell runs, producing 2x151bp paired-end reads. Demultiplexing, quality control and adapter trimming was performed with bcl-convert1 (v4.1.5).

Illumina and Nanopore combo assembly and annotation: Porechop[78] (version 0.2.4; default parameters) was used to trim residual adapter sequence from the Oxford Nanopore Technology (ONT) reads that may have been missed during basecalling and demultiplexing.

De novo genome assemblies were generated from the Oxford Nanopore Technologies (ONT) read data with Flye[79] (version 2.9.2) under the nano-hq (ONT high-quality reads) model. Additional Flye options initiate the assembly by first using reads longer than an estimated N50 based on a genome size of 6Mbp. Subsequent polishing used the Illumina read data with Pilon[80] (version 2.5.1) under default parameters. To reduce erroneous assembly artifacts caused by low quality nanopore reads, long read contigs with an average short read coverage of 15x or less were removed from the assembly.

Assembled contigs were evaluated for circularization via circulator[82] (version 1.5.5) using the ONT long reads. Assembly annotation was then performed with Bakta[81] (version 1.8.1) using the Bakta v5 database. Finally, assembly statistics were recorded with QUAST[83] (version 5.2.0).

ILA detection via liquid chromatography mass spectrometry (LCMS)

Bacterial cell free supernatants: Cell free supernatant was obtained from *L. murinus* KD6 and *L. reuteri* strain ATCC23272 24 h anaerobic cultures in BHI^{CHV}. Cell free supernatants (CFS) were collected where cultures were pelleted via centrifugation at 3,500 rpm, for 10 min and then the resulting supernatant was passed through a 0.22 μm filter and stored at −80°C.

CFS extraction for LCMS: To assess ILA production CFS were extracted with acetonitrile (ACN) and methanol (MeOH) where 250 μL of CFS was aliquoted and 1 mL of a 50:50 ACN:MeOH was added. 100 pg/μL of a stable isotope labeled amino acid mixture for mass spec (Sigma Aldrich; cat#909653) and 2-Amino-3-bromo-5-methylbenzoic acid was added to each sample and vortexed briefly. Samples were then incubated on ice for 15 min then centrifuged at max speed at 4°C on a tabletop centrifuge and resulting supernatants were transferred to a new tube. Samples were then dried with a speedvac and resuspended in 200 μL LCMS grade water.

Fecal extraction for LCMS: Fecal samples from HFD, HFD-KE, or a KD fed SJL/J mice EAE on days 7, 21, and 28 days post disease induced were used to quantify ILA. Frozen stool samples were and lyophilized (−50 C at 260 mtorr) to dryness for 65 h. Lyophilized stool samples were transferred to Precellys homogenization tubes (P000911-LYSK0-A) and homogenized using Precellys 24-bead homogenizer pre-cooled with dry ice at 6400 rpm, 3 × 20s with 30s of rest. 1 mL of acetonitrile:methanol:water (1:1:1) + 1% formic acid with an internal standard mix of ^{13}C, ^{15}N labeled amino acids (Sigma, cat #767946) at 100 pg/L was added to homogenized samples, briefly vortexed and allowed to stand at 4° C for 30 min. Samples were centrifuged at 21,130 rcf for 15 min, then supernatants were transferred to new eppendorf tubes and dried under vacuum. Samples were stored at 20° C or below until analysis. Prior to injection, samples were resuspended in water (100 μl), vortexed, and centrifuged to remove particulates. Resulting supernatants were then diluted 10-fold and transferred to UPLC vial containing 200 μl glass inserts.

Targeted metabolomics: Samples were analyzed using an SCIEX ExionLC UPLC in series with SCIEX 7500 Triplequadrupole. 5 μL of each sample were injected and separated using

Phenomenex's Kinetex 2.6 mm F5 100 Å LC column 2.1 × 150 mm (cat # 00F-4723-AN). The mobile phase scheme consisted of A: H_2O + 0.01% formic acid and B: Acetonitrile +0.01% formic acid. At a constant flow rate of 200 mL/min, metabolites were separated using the following gradient: 0.2% B (initial), 0.2% B (2 min), 5% B (5 min), 25% B (11 min), 98% B (13 min), 98% B (16 min), 0.2% B (16.1 min), and 0.2% B (20 min). Data was acquired in positive mode with optimized MRM pair determined from a commercial standard. The following source parameters were used: Ion source gas 1 = 45, Ion source gas 2 = 70, CUR = 40, CAD = 9, TEM = 375, Ion Source = 2000, and pause time = 5 ms. The following MRM pairs were used: 3-Indolelactic acid - Q1 = 206.1, Q3 = 188.1, CE = 20, $^{15}N_2$-Tryptophan - Q1 = 207.2, Q3 = 147.1, CE = 20. EP and CXP values were held at 10 and 15 and dwell time = 5 ms for both MRM pairs. For the ILA quantification of ILA in fecal samples, a standard curve of ILA was used for quantification and the levels were normalized to fecal weight. The following compound parameters were used: Indole 3-lactic acid – Q1 206.178 m/z, Q3 187.972 m/z, CE = 20, Dwell time 5 ms, EP = 10, CXP = 10.

Data analysis: Raw data was processed using SCIEX OS software suite (version 2.16.59781) for analyte peak integration and quantitation. A freshly prepared 6-point standard curve of indole 3-lactic acid ranging from 0.005–1 ng ran in duplicate was used to determine the amount of indole 3-lactic acid detected. Data was normalized by lyophilized stool weight.

Th17 skewing assay—Th17 skewing was performed as described.[48] RBC lysed mouse splenocytes from a male C57BL/6J CONV-R 17-week-old mouse were filtered through a 40 μm filter and used for T cell isolation. Naive $CD4^+$ T cells were isolated via Dynabeads untouched mouse CD4 isolation kit (ThermoFisher) according to kit specifications. In a 96 well plate pre-coated with anti-CD3 (5 μg/mL, overnight 37°C), equal cell numbers were plated and were treated with CFS or media controls at 5% v/v. At the same time, Th17 skewing conditions were supplied: 10 μg/mL anti-CD28, 0.3 ng/mL TGFbeta, 20 ng/mL IL-6, 2 ng/mL anti-IFNgamma, and 2 ng/mL anti-IL-4.[49] Isolated $CD4^+$ T cells were developed in Th17 skewing conditions with bacterial CFS present for 4 days at 37°C and then restimulated with a cell stimulation cocktail (Fisher Scientific) containing PMA and ionomycin, according to the manufacturer's instructions. Cells were restimulated at 37°C overnight and then supernatants were harvested for IL-17a quantification via ELISA. We utilized the mouse IL-17a (homodimer) ELISA (ThermoFisher) according to the kit instructions, where 100 μL of cell culture media was loaded onto the ELISA. Absorbance for ELISA was measured at 450 nm and the blank background signal was subtracted.

DNA extraction—Mouse fecal samples (30–60 mg of preweighed material) were homogenized with bead beating for 5 min (Mini-Beadbeater-96, BioSpec) using the ZR BashingBead lysis matrix containing 0.1 and 0.5 mm beads (ZR-96 BashingBead Lysis Rack, Zymo Research; cat# S6012-50) and the lysis solution provided in the ZymoBIOMICS 96 MagBead DNA Kit (Zymo Research; cat# D4302). Bead beating was repeated for a total of three 5 min rounds with 5 min incubation at room temperature in between. Samples were then incubated at 65°C for 10 min before centrifuging for 5 min at 4,000 rpm. The supernatant was transferred to 1 mL deep-well plates and the DNA was then

purified using the ZymoBIOMICS 96 MagBead DNA Kit according to the manufacturer's instructions.

16S rRNA gene sequencing—The V4 region of the 16S rRNA gene was amplified using primers 515F and 806R (see key resources table). The reaction mix was: 0.45 μL DMSO for PCR (Sigma; cat# D8418-50 mL), 0.0045 μL SYBR Green I (Sigma; cat# S9430) 10x diluted in DMSO to 1000x, KAPA HiFi PCR kit (1.8 μL 5x KAPA HiFi Buffer, 0.27 μL 10 mM dNTPs, 0.18 μL KAPA HiFi polymerase; cat# KK2502), 0.045 μL of each of the amplification primers 515F and 806R (final concentration 1 μM), 6.2055 μL Nuclease-free H2O (Life Tech; cat# 0977-023) and 1 μL DNA. We used a BioRad CFX 384 real-time PCR instrument with four serial 10-fold dilutions of extracted DNA template (10–100 ng/μL). Amplification was as follows: 5 min at 95°C, 20x (20 s at 98°C, 15 s at 55°C, 60 s at 72°C), and hold at 4°C. Individual sample dilutions with amplification in the exponential phase (non-plateaued) were selected for subsequent indexing PCR using dual GoLay index primers.[93] For indexing KAPA HiFi PCR kit was used with, 4 μL 5x KAPA HiFi Buffer, 0.6 μL 10 mM dNTPs, 1 μL DMSO, 0.4 μL KAPA HiFi polymerase, 4 μL of indexing primer,[93] and 10 μL of 100-fold dilution of a non-plateaued primary PCR reaction was used with the same amplification as above. Amplicons were quantified with PicoGreen (Quant-It dsDNA, Life Technologies; cat# P11496) according to manufacturer's instructions and pooled at equimolar concentrations. Aliquots of the pools were then column (MinElute PCR Purification Kit, QIAGEN; cat# 28004) and gel purified (QIAquick Gel Extraction Kit, QIAGEN; cat# 28704). Libraries were then quantified using KAPA Library Quantification Kit for Illumina Platforms (KAPA; cat# KK4824) according to manufacturer's instructions and sequenced with an Illumina MiSeqV3 using 15% PhiX spike in. All sequencing was paired end, with 270 bp fragments, index length of 8 bp, mean library size 435 bp.

16S rRNA gene analysis—Primer sequences and adapters were trimmed using the cutadapt plugin in QIIME2,[74] and were truncated to 220 base pairs for forward sequences and 150 bp for reverse sequences. Sequences then underwent quality filtering, denoising, and chimera filtering utilizing DADA2 (dada2 v 1.18.0),[77] using default parameters (QIIME command PairedEndFastqManifestPhred33). Taxonomy was assigned to amplicon sequence variants (ASVs) using the SILVA v138 database.[75] Sequence variants were filtered such that they were present in >3 samples with ≥10 reads using MicrobeR (version 0.3.2).[94] Data was then transformed using a Centered log2-ratio (CLR) with a CZM pseudocount replacement by zCompositions version 1.4.0–1.[95] CLR data was transformed into a Euclidean distance matrix using the dist command from the stats package in R (version 4.2.1). PERMANOVA testing was conducted on this distance matrix using adonis2 and Shannon diversity was calculated using the diversity command from vegan (version 2.6.4).[96] Filtered counts were used in differential abundance. Differential abundance testing of ASVs was completed using ALDEx2.[76] A phylogenetic tree of statistically significant features was created using the ggtree package version 3.6.2.[97]

***Ex vivo* incubation and sequencing of human stool samples analysis—**We re-analyzed data from Ang et al. 2020[16] to assess changes in ILA-producing microbes in human *ex vivo* communities exposed to beta-hydroxybutyrate. *Ex vivo* communities

were generated from human fecal samples and incubated for 24 h in BHI^{CHV} media in the presence or absence of 12.5 mM beta-hydroxybutyrate in quadruplet, followed by DNA extraction and 16S rRNA sequencing as described.[16] Demultiplexed sequences were processed with a 16S rRNA gene analysis pipeline and mapped to species abundances with qiime2R and phyloseq as described.[98] Relative abundances of strains with documented ILA production (≥4 fold-change over controls),[56] were binned and compared using the mixed-effects model Abundance ~Treatment + 1|Donor using the nlme package.[99]

ILA-producer analysis in iMSMS—We downloaded patient metadata and the ASV read table from the iMSMS consortium.[26] We reassigned taxonomy based on SILVA SSU database 138 in RStudio and normalized as proportions. Using these data, relative abundances of strains with documented ILA production (≥4 fold-change over controls)[56] were assessed. ILA-producing species proportions were summed and converted to percentage of total ASVs. We binned multiple sclerosis severity based on EDSS, a standardized disease scoring rubric for multiple sclerosis, with EDSS 0–3.5 classified as mild, EDSS 4–6.5 (severe disability, highly ambulatory) classified as moderate, and EDSS 7–9.5 (wheelchair bound) classified as severe.

Growth curves of L. *murinus* KD6 and *B. adolescentis* BD1—A 96 well plate was filled with 150 μL of BHI supplemented with L-cysteine (0.05% w/v) and resazurin (0.0001%, w/v) (BHI^{CR}) and 7 colonies of *L. murinus* KD6 and *B. adolescentis* BD1 were grown overnight. 1.5 μL of these turbid cultures was used as starter cultures into 150 μL BHI^{CR} with three concentrations of βHB (Sigma 166898) - 0 mM, 12.5 mM, and 50 mM from a 0.22 μM sterile filtered 1M solution of βHB made in BHI^{CR}. This was then loaded onto the EON plate reader, set with continuous shaking and OD every 15 min. For background blank subtraction, multiple replicates of 0 mM, 12.5 mM, and 50 mM βHB concentrations in BHI^{CR} were used. For 1 biological replicate of the *B. adolescentis* BD1 50 mM condition, growth metrics could not be measured due to a poor model fit using the Growthcurver tool[84] (R package growthcurver 0.3.1).

QUANTIFICATION AND STATISTICAL ANALYSIS

Statistical tests, the software used, the number of replicates, definitions of center, and dispersion/precision measures are specified in the figure legends or on the plots themselves where possible. Tests were two-tailed unless otherwise noted. Statistical analyses were performed using GraphPad Prism software (Version 8), QIIME2, and R. Categorical data across 3 or more experimental groups was analyzed using ANOVA Kruskal-Wallis with Dunn's multiple comparison test and one-way ANOVA with Dunnett's multiple comparisons test for comparisons to BHI^{CHV} control in Th17 skewing assay. Unpaired Welch's *t*-tests were used for comparisons of two groups. Longitudinal data was analyzed using two-way ANOVA. For 16S rRNA gene analysis, PERMANOVA testing was conducted on this distance matrix using adonis2. For correlations, Spearman correlations were performed with the exception of the correlation between ΔCLR HFD-KE vs. HFD and DCLR KD vs. HFD which is a Pearson correlation due to the type of data being matched between axes.

Supplementary Material

Refer to Web version on PubMed Central for supplementary material.

ACKNOWLEDGMENTS

We would like to acknowledge the UCSF Gnotobiotics Core Facility (gnotobiotics.ucsf.edu) and the Parnassus Flow Cytometry CoLab RRID:SCR_018206 supported in part by the DRC grant NIH P30 DK063720. We also acknowledge the UCSF Quantitative Metabolite Analysis Center for their help quantifying ILA levels. We thank Dr. Michael Kattah for generously donating the VillinER/Cre mice. We thank BHB Therapeutics for providing the ketone ester. Funding was provided from the National Institutes of Health: R01DK114034, R01HL122593, R01AR074500, and R01AT011117 to P.J.T.; F32AI14745601, K99AI159227, and R00AI159227-03 to M.A.; K08HL165106 to V.U.; K08AR073930 to D.O. and R.R.N; R01AG067333 to J.C.N.; and R01DK091538 and R01AG069781 to P.A.C. P.J.T is a Chan Zuckerberg Biohub-San Francisco Investigator and was a Nadia's Gift Foundation Innovator supported, in part, by the Damon Runyon Cancer Research Foundation (DRR4216). Model figures were created with BioRender.com.

REFERENCES

1. Sanchez JMS, DePaula-Silva AB, Libbey JE, and Fujinami RS (2022). Role of diet in regulating the gut microbiota and multiple sclerosis. Clin. Immunol 235, 108379. [PubMed: 32156562]
2. Fitzpatrick JA, Melton SL, Yao CK, Gibson PR, and Halmos EP (2022). Dietary management of adults with IBD - the emerging role of dietary therapy. Nat. Rev. Gastroenterol. Hepatol 19, 652–669. [PubMed: 35577903]
3. Zmora N, Suez J, and Elinav E (2019). You are what you eat: diet, health and the gut microbiota. Nat. Rev. Gastroenterol. Hepatol 16, 35–56. [PubMed: 30262901]
4. Vieira SM, Pagovich OE, and Kriegel MA (2014). Diet, microbiota and autoimmune diseases. Lupus 23, 518–526. [PubMed: 24763536]
5. Thorburn AN, Macia L, and Mackay CR (2014). Diet, metabolites, and "western-lifestyle" inflammatory diseases. Immunity 40, 833–842. [PubMed: 24950203]
6. Brenton JN, Banwell B, Bergqvist AC, Lehner-Gulotta D, Gampper L, Leytham E, Coleman R, and Goldman MD (2019). Pilot study of a ketogenic diet in relapsing-remitting MS. Neurol. Neuroimmunol. Neuroinflamm 6, e565. [PubMed: 31089482]
7. Brenton JN, Lehner-Gulotta D, Woolbright E, Banwell B, Bergqvist AGC, Chen S, Coleman R, Conaway M, and Goldman MD (2022). Phase II study of ketogenic diets in relapsing multiple sclerosis: safety, tolerability and potential clinical benefits. J. Neurol. Neurosurg. Psychiatry 93, 637–644. [PubMed: 35418509]
8. Storoni M, and Plant GT (2015). The Therapeutic Potential of the Ketogenic Diet in Treating Progressive Multiple Sclerosis. Mult. Scler. Int 2015, 681289. [PubMed: 26839705]
9. Choi IY, Piccio L, Childress P, Bollman B, Ghosh A, Brandhorst S, Suarez J, Michalsen A, Cross AH, Morgan TE, et al. (2016). A Diet Mimicking Fasting Promotes Regeneration and Reduces Autoimmunity and Multiple Sclerosis Symptoms. Cell Rep. 15, 2136–2146. [PubMed: 27239035]
10. Kim DY, Hao J, Liu R, Turner G, Shi F-D, and Rho JM (2012). Inflammation-mediated memory dysfunction and effects of a ketogenic diet in a murine model of multiple sclerosis. PLoS One 7, e35476. [PubMed: 22567104]
11. Lin W-S, Lin S-J, Liao P-Y, Suresh D, Hsu T-R, and Wang P-Y (2022). Role of Ketogenic Diets in Multiple Sclerosis and Related Animal Models: An Updated Review. Adv. Nutr 13, 2002–2014. [PubMed: 35679067]
12. Puchalska P, and Crawford PA (2021). Metabolic and Signaling Roles of Ketone Bodies in Health and Disease. Annu. Rev. Nutr 41, 49–77. [PubMed: 34633859]
13. Goldberg EL, Asher JL, Molony RD, Shaw AC, Zeiss CJ, Wang C, Morozova-Roche LA, Herzog RI, Iwasaki A, and Dixit VD (2017). β-Hydroxybutyrate Deactivates Neutrophil NLRP3 Inflammasome to Relieve Gout Flares. Cell Rep. 18, 2077–2087. [PubMed: 28249154]

14. Puchalska P, Martin SE, Huang X, Lengfeld JE, Daniel B, Graham MJ, Han X, Nagy L, Patti GJ, and Crawford PA (2019). Hepatocyte-Macrophage Acetoacetate Shuttle Protects against Tissue Fibrosis. Cell Metabol. 29, 383–398.e7.
15. Karagiannis F, Peukert K, Surace L, Michla M, Nikolka F, Fox M, Weiss P, Feuerborn C, Maier P, Schulz S, et al. (2022). Impaired ketogenesis ties metabolism to T cell dysfunction in COVID-19. Nature 609, 801–807. [PubMed: 35901960]
16. Ang QY, Alexander M, Newman JC, Tian Y, Cai J, Upadhyay V, Turnbaugh JA, Verdin E, Hall KD, Leibel RL, et al. (2020). Ketogenic Diets Alter the Gut Microbiome Resulting in Decreased Intestinal Th17 Cells. Cell 181, 1263–1275.e16. [PubMed: 32437658]
17. Olson CA, Vuong HE, Yano JM, Liang QY, Nusbaum DJ, and Hsiao EY (2018). The Gut Microbiota Mediates the Anti-Seizure Effects of the Ketogenic Diet. Cell 174, 497. [PubMed: 30007420]
18. Lindefeldt M, Eng A, Darban H, Bjerkner A, Zetterström CK, Al-lander T, Andersson B, Borenstein E, Dahlin M, and Prast-Nielsen S (2019). The ketogenic diet influences taxonomic and functional composition of the gut microbiota in children with severe epilepsy. NPJ Biofilms Microbiomes 5, 5. [PubMed: 30701077]
19. Mardinoglu A, Wu H, Bjornson E, Zhang C, Hakkarainen A, Räsänen SM, Lee S, Mancina RM, Bergentall M, Pietiläinen KH, et al. (2018). An Integrated Understanding of the Rapid Metabolic Benefits of a Carbohydrate-Restricted Diet on Hepatic Steatosis in Humans. Cell Metabol. 27, 559–571.e5.
20. Constantinescu CS, Farooqi N, O'Brien K, and Gran B (2011). Experimental autoimmune encephalomyelitis (EAE) as a model for multiple sclerosis (MS). Br. J. Pharmacol 164, 1079–1106. [PubMed: 21371012]
21. Ransohoff RM (2012). Animal models of multiple sclerosis: the good, the bad and the bottom line. Nat. Neurosci 15, 1074–1077. [PubMed: 22837037]
22. Lee YK, Menezes JS, Umesaki Y, and Mazmanian SK (2011). Proinflammatory T-cell responses to gut microbiota promote experimental autoimmune encephalomyelitis. Proc. Natl. Acad. Sci. USA 108, 4615–4622. [PubMed: 20660719]
23. Cekanaviciute E, Yoo BB, Runia TF, Debelius JW, Singh S, Nelson CA, Kanner R, Bencosme Y, Lee YK, Hauser SL, et al. (2017). Gut bacteria from multiple sclerosis patients modulate human T cells and exacerbate symptoms in mouse models. Proc. Natl. Acad. Sci. USA 114, 10713–10718. [PubMed: 28893978]
24. Miyauchi E, Kim S-W, Suda W, Kawasumi M, Onawa S, Taguchi-Atarashi N, Morita H, Taylor TD, Hattori M, and Ohno H (2020). Gut microorganisms act together to exacerbate inflammation in spinal cords. Nature 585, 102–106. [PubMed: 32848245]
25. Berer K, Gerdes LA, Cekanaviciute E, Jia X, Xiao L, Xia Z, Liu C, Klotz L, Stauffer U, Baranzini SE, et al. (2017). Gut microbiota from multiple sclerosis patients enables spontaneous autoimmune encephalomyelitis in mice. Proc. Natl. Acad. Sci. USA 114, 10719–10724. [PubMed: 28893994]
26. iMSMS Consortium (2022). Gut microbiome of multiple sclerosis patients and paired household healthy controls reveal associations with disease risk and course. Cell 185, 3467–3486.e16. [PubMed: 36113426]
27. Aranda-Díaz A, Ng KM, Thomsen T, Real-Ramírez I, Dahan D, Dittmar S, Gonzalez CG, Chavez T, Vasquez KS, Nguyen TH, et al. (2022). Establishment and characterization of stable, diverse, fecal-derived in vitro microbial communities that model the intestinal microbiota. Cell Host Microbe 30, 260–272.e5. [PubMed: 35051349]
28. Liu C, Zhang N, Zhang R, Jin L, Petridis AK, Loers G, Zheng X, Wang Z, and Siebert H-C (2020). Cuprizone-Induced Demyelination in Mouse Hippocampus Is Alleviated by Ketogenic Diet. J. Agric. Food Chem 68, 11215–11228. [PubMed: 32921051]
29. Zhang N, Liu C, Zhang R, Jin L, Yin X, Zheng X, Siebert H-C, Li Y, Wang Z, Loers G, and Petridis AK (2020). Amelioration of clinical course and demyelination in the cuprizone mouse model in relation to ketogenic diet. Food Funct. 11, 5647–5663. [PubMed: 32539054]
30. Stromnes IM, and Goverman JM (2006). Active induction of experimental allergic encephalomyelitis. Nat. Protoc 1, 1810–1819. [PubMed: 17487163]

31. Hirota K, Duarte JH, Veldhoen M, Hornsby E, Li Y, Cua DJ, Ahlfors H, Wilhelm C, Tolaini M, Menzel U, et al. (2011). Fate mapping of IL-17-producing T cells in inflammatory responses. Nat. Immunol 12, 255–263. [PubMed: 21278737]
32. Stubbs BJ, Koutnik AP, Goldberg EL, Upadhyay V, Turnbaugh PJ, Verdin E, and Newman JC (2020). Investigating Ketone Bodies as Immunometabolic Countermeasures against Respiratory Viral Infections. Méd. 1, 43–65. [PubMed: 32838361]
33. Youm Y-H, Nguyen KY, Grant RW, Goldberg EL, Bodogai M, Kim D, D'Agostino D, Planavsky N, Lupfer C, Kanneganti TD, et al. (2015). The ketone metabolite β-hydroxybutyrate blocks NLRP3 inflammasome-mediated inflammatory disease. Nat. Med 21, 263–269. [PubMed: 25686106]
34. Singh V, Yeoh BS, Walker RE, Xiao X, Saha P, Golonka RM, Cai J, Bretin ACA, Cheng X, Liu Q, et al. (2019). Microbiota fermentation-NLRP3 axis shapes the impact of dietary fibres on intestinal inflammation. Gut 68, 1801–1812. [PubMed: 30670576]
35. Goldberg EL, Molony RD, Kudo E, Sidorov S, Kong Y, Dixit VD, and Iwasaki A (2019). Ketogenic diet activates protective γδ T cell responses against influenza virus infection. Sci. Immunol 4, eaav2026. [PubMed: 31732517]
36. Yurista SR, Matsuura TR, Silljé HHW, Nijholt KT, McDaid KS, Shewale SV, Leone TC, Newman JC, Verdin E, van Veldhuisen DJ, et al. (2021). Ketone Ester Treatment Improves Cardiac Function and Reduces Pathologic Remodeling in Preclinical Models of Heart Failure. Circ. Heart Fail 14, e007684. [PubMed: 33356362]
37. Terry RL, Ifergan I, and Miller SD (2016). Experimental Autoimmune Encephalomyelitis in Mice. Methods Mol. Biol 1304, 145–160. [PubMed: 25005074]
38. Hooke - Protocols - EAE Induction by Active Immunization in SJL mice https://hookelabs.com/protocols/eaeAI_SJL.html.
39. Dashti N, and Ontko JA (1979). Rate-limiting function of 3-hydroxy-3-methylglutaryl-coenzyme A synthase in ketogenesis. Biochem. Med 22, 365–374. [PubMed: 93966]
40. Newman JC, and Verdin E (2017). β-Hydroxybutyrate: A Signaling Metabolite. Annu. Rev. Nutr 37, 51–76. [PubMed: 28826372]
41. Rakoff-Nahoum S, Paglino J, Eslami-Varzaneh F, Edberg S, and Medzhitov R (2004). Recognition of commensal microflora by toll-like receptors is required for intestinal homeostasis. Cell 118, 229–241. [PubMed: 15260992]
42. Ochoa-Repáraz J, Mielcarz DW, Ditrio LE, Burroughs AR, Foureau DM, Haque-Begum S, and Kasper LH (2009). Role of gut commensal microflora in the development of experimental autoimmune encephalomyelitis. J. Immunol 183, 6041–6050. [PubMed: 19841183]
43. Chu F, Shi M, Lang Y, Shen D, Jin T, Zhu J, and Cui L (2018). Gut Microbiota in Multiple Sclerosis and Experimental Autoimmune Encephalomyelitis: Current Applications and Future Perspectives. Mediat. Inflamm 2018, 8168717.
44. McGinley AM, Sutton CE, Edwards SC, Leane CM, DeCourcey J, Teijeiro A, Hamilton JA, Boon L, Djouder N, and Mills KH (2020). Interleukin-17A Serves a Priming Role in Autoimmunity by Recruiting IL-1β-Producing Myeloid Cells that Promote Pathogenic T Cells. Immunity 52, 342–356.e6. [PubMed: 32023490]
45. Haak S, Croxford AL, Kreymborg K, Heppner FL, Pouly S, Becher B, and Waisman A (2009). IL-17A and IL-17F do not contribute vitally to autoimmune neuro-inflammation in mice. J. Clin. Invest 119, 61–69. [PubMed: 19075395]
46. Komiyama Y, Nakae S, Matsuki T, Nambu A, Ishigame H, Kakuta S, Sudo K, and Iwakura Y (2006). IL-17 plays an important role in the development of experimental autoimmune encephalomyelitis. J. Immunol 177, 566–573. [PubMed: 16785554]
47. Cosorich I, Dalla-Costa G, Sorini C, Ferrarese R, Messina MJ, Dolpady J, Radice E, Mariani A, Testoni PA, Canducci F, et al. (2017). High frequency of intestinal TH17 cells correlates with microbiota alterations and disease activity in multiple sclerosis. Sci. Adv 8, e1700492.
48. Alexander M, Ang QY, Nayak RR, Bustion AE, Sandy M, Zhang B, Upadhyay V, Pollard KS, Lynch SV, and Turnbaugh PJ (2022). Human gut bacterial metabolism drives Th17 activation and colitis. Cell Host Microbe 80, 17–30.e9.

49. Huh JR, Leung MWL, Huang P, Ryan DA, Krout MR, Malapaka RRV, Chow J, Manel N, Ciofani M, Kim SV, et al. (2011). Digoxin and its derivatives suppress TH17 cell differentiation by antagonizing RORγt activity. Nature 472, 486–490. [PubMed: 21441909]
50. Montgomery TL, Eckstrom K, Lile KH, Caldwell S, Heney ER, Lahue KG, D'Alessandro A, Wargo MJ, and Krementsov DN (2022). Lactobacillus reuteri tryptophan metabolism promotes host susceptibility to CNS autoimmunity. Microbiome 10, 198. [PubMed: 36419205]
51. Wilck N, Matus MG, Kearney SM, Olesen SW, Forslund K, Bartolomaeus H, Haase S, Mähler A, Balogh A, Markó L, et al. (2017). Salt-responsive gut commensal modulates TH17 axis and disease. Nature 551, 585–589. [PubMed: 29143823]
52. Agus A, Planchais J, and Sokol H (2018). Gut Microbiota Regulation of Tryptophan Metabolism in Health and Disease. Cell Host Microbe 28, 716–724.
53. Pan T, Pei Z, Fang Z, Wang H, Zhu J, Zhang H, Zhao J, Chen W, and Lu W (2023). Uncovering the specificity and predictability of tryptophan metabolism in lactic acid bacteria with genomics and metabolomics. Front. Cell. Infect. Microbiol 18, 1154346.
54. Dodd D, Spitzer MH, Van Treuren W, Merrill BD, Hryckowian AJ, Higginbottom SK, Le A, Cowan TM, Nolan GP, Fischbach MA, and Sonnenburg JL (2017). A gut bacterial pathway metabolizes aromatic amino acids into nine circulating metabolites. Nature 551, 648–652. [PubMed: 29168502]
55. Cervantes-Barragan L, Chai JN, Tianero MD, Di Luccia B, Ahern PP, Merriman J, Cortez VS, Caparon MG, Donia MS, Gilfillan S, et al. (2017). Lactobacillus reuteri induces gut intraepithelial CD4+CD8αα+ T cells. Science 857, 806–810.
56. Han S, Van Treuren W, Fischer CR, Merrill BD, DeFelice BC, Sanchez JM, Higginbottom SK, Guthrie L, Fall LA, Dodd D, et al. (2021). A metabolomics pipeline for the mechanistic interrogation of the gut microbiome. Nature 595, 415–420. [PubMed: 34262212]
57. Fitzgerald KC, Smith MD, Kim S, Sotirchos ES, Kornberg MD, Douglas M, Nourbakhsh B, Graves J, Rattan R, Poisson L, et al. (2021). Multi-omic evaluation of metabolic alterations in multiple sclerosis identifies shifts in aromatic amino acid metabolism. Cell Rep. Med 2, 100424. [PubMed: 34755135]
58. Levi I, Gurevich M, Perlman G, Magalashvili D, Menascu S, Bar N, Godneva A, Zahavi L, Chermon D, Kosower N, et al. (2021). Potential role of indolelactate and butyrate in multiple sclerosis revealed by integrated microbiome-metabolome analysis. Cell Rep. Med 2, 100246. [PubMed: 33948576]
59. Batch JT, Lamsal SP, Adkins M, Sultan S, and Ramirez MN (2020). Advantages and Disadvantages of the Ketogenic Diet: A Review Article. Cureus 12, e9639. [PubMed: 32923239]
60. Ochoa-Repáraz J, Mielcarz DW, Ditrio LE, Burroughs AR, Begum-Haque S, Dasgupta S, Kasper DL, and Kasper LH (2010). Central nervous system demyelinating disease protection by the human commensal Bacteroides fragilis depends on polysaccharide A expression. J. Immunol 185, 4101–4108. [PubMed: 20817872]
61. Cignarella F, Cantoni C, Ghezzi L, Salter A, Dorsett Y, Chen L, Phillips D, Weinstock GM, Fontana L, Cross AH, et al. (2018). Intermittent Fasting Confers Protection in CNS Autoimmunity by Altering the Gut Microbiota. Cell Metabol. 27, 1222–1235.e6.
62. Fitzgerald KC, Bhargava P, Smith MD, Vizthum D, Henry-Barron B, Kornberg MD, Cassard SD, Kapogiannis D, Sullivan P, Baer DJ, et al. (2022). Intermittent calorie restriction alters T cell subsets and metabolic markers in people with multiple sclerosis. EBioMedicine 82,104124. [PubMed: 35816900]
63. Piccio L, Stark JL, and Cross AH (2008). Chronic calorie restriction attenuates experimental autoimmune encephalomyelitis. J. Leukoc. Biol. 84, 940–948. [PubMed: 18678605]
64. Mirzaei V, Eidi A, Manaheji H, Oryan S, and Zaringhalam J (2021). B-hydroxybutyrate attenuates clinical symptoms and pain behaviors in MOG-induced encephalomyelitis. Neurochem. J 15, 181–186.
65. Swidsinski A, Dörffel Y, Loening-Baucke V, Gille C, Göktas Ö, Reißhauer A, Neuhaus J, Weylandt K-H, Guschin A, and Bock M (2017). Reduced Mass and Diversity of the Colonic Microbiome in Patients with Multiple Sclerosis and Their Improvement with Ketogenic Diet. Front. Microbiol 8, 1141. [PubMed: 28702003]

66. Levy M, Thaiss CA, Zeevi D, Dohnalová L, Zilberman-Schapira G, Mahdi JA, David E, Savidor A, Korem T, Herzig Y, et al. (2015). Microbiota-Modulated Metabolites Shape the Intestinal Microenvironment by Regulating NLRP6 Inflammasome Signaling. Cell 168, 1428–1443.

67. Elinav E, Strowig T, Kau AL, Henao-Mejia J, Thaiss CA, Booth AJ, Peaper DR, Bertin J, Eisenbarth SC, Gordon JI, and Flavell R (2011). NLRP6 inflammasome regulates colonic microbial ecology and risk for colitis. Cell 145, 745–757. [PubMed: 21565393]

68. Cheng C-W, Biton M, Haber AL, Gunduz N, Eng G, Gaynor LT, Tripathi S, Calibasi-Kocal G, Rickelt S, Butty VL, et al. (2019). Ketone Body Signaling Mediates Intestinal Stem Cell Homeostasis and Adaptation to Diet. Cell 178, 1115–1131.e15. [PubMed: 31442404]

69. Achanta LB, and Rae CD (2017). B-Hydroxybutyrate in the brain: One molecule, multiple mechanisms. Neurochem. Res 42, 35–49. [PubMed: 27826689]

70. Gutiérrez-Vázquez C, and Quintana FJ (2018). Regulation of the Immune Response by the Aryl Hydrocarbon Receptor. Immunity 48, 19–33. [PubMed: 29343438]

71. Ehrlich AM, Pacheco AR, Henrick BM, Taft D, Xu G, Huda MN, Mishchuk D, Goodson ML, Slupsky C, Barile D, et al. (2020). Indole-3-lactic acid associated with Bifidobacterium-dominated microbiota significantly decreases inflammation in intestinal epithelial cells. BMC Microbiol. 20, 357. [PubMed: 33225894]

72. Veldhoen M, Hirota K, Westendorf AM, Buer J, Dumoutier L, Renauld J-C, and Stockinger B (2008). The aryl hydrocarbon receptor links TH17-cell-mediated autoimmunity to environmental toxins. Nature 458, 106–109.

73. Brockmann L, Tran A, Huang Y, Edwards M, Ronda C, Wang HH, and Ivanov II (2023). Intestinal microbiota-specific Th17 cells possess regulatory properties and suppress effector T cells via c-MAF and IL-10. Immunity 56, 2719–2735.e7. [PubMed: 38039966]

74. Bolyen E, Rideout JR, Dillon MR, Bokulich NA, Abnet CC, Al-Ghalith GA, Alexander H, Alm EJ, Arumugam M, Asnicar F, et al. (2019). Reproducible, interactive, scalable and extensible microbiome data science using QIIME 2. Nat. Biotechnol 87, 852–857.

75. Quast C, Pruesse E, Yilmaz P, Gerken J, Schweer T, Yarza P, Peplies J, and Glöckner FO (2012). The SILVA ribosomal RNA gene database project: improved data processing and web-based tools. Nucleic Acids Res. 41, D590–D596. [PubMed: 23193283]

76. Gloor G, Fernandes A, Macklaim J, Albert A, Links M, Quinn T, Wu JR, Wong RG, and Lieng B (2019). ALDEx2 package: Analysis of differential abundance taking sample variation into account. Preprint at Bioconductor. https://rdrr.io/bioc/ALDEx2/.

77. Callahan BJ, McMurdie PJ, Rosen MJ, Han AW, Johnson AJA, and Holmes SP (2016). DADA2: High-resolution sample inference from Illumina amplicon data. Nat. Methods 13, 581–583. [PubMed: 27214047]

78. Wick R. Porechop: adapter trimmer for Oxford Nanopore reads (Github) https://github.com/rrwick/Porechop.

79. Kolmogorov M, Yuan J, Lin Y, and Pevzner PA (2019). Assembly of long, error-prone reads using repeat graphs. Nat. Biotechnol 37, 540–546. [PubMed: 30936562]

80. Walker BJ, Abeel T, Shea T, Priest M, Abouelliel A, Sakthikumar S, Cuomo CA, Zeng Q, Wortman J, Young SK, and Earl AM (2014). Pilon: an integrated tool for comprehensive microbial variant detection and genome assembly improvement. PLoS One 9, e112963. [PubMed: 25409509]

81. Schwengers O, Jelonek L, Dieckmann MA, Beyvers S, Blom J, and Goesmann A (2021). Bakta: rapid and standardized annotation of bacterial genomes via alignment-free sequence identification. Microb. Genom 7, 000685. 10.1099/mgen.0.000685. [PubMed: 34739369]

82. Hunt M, Silva ND, Otto TD, Parkhill J, Keane JA, and Harris SR (2015). Circlator: automated circularization of genome assemblies using long sequencing reads. Genome Biol. 16, 294. [PubMed: 26714481]

83. Gurevich A, Saveliev V, Vyahhi N, and Tesler G (2013). QUAST: quality assessment tool for genome assemblies. Bioinformatics 29, 1072–1075. [PubMed: 23422339]

84. Sprouffske K, and Wagner A (2016). Growthcurver: an R package for obtaining interpretable metrics from microbial growth curves. BMC Bioinf. 17, 172.

85. el Marjou F, Janssen K-P, Hung-Junn Chang B, Li M, Hindie V, Chan L, Louvard D, Chambon P, Metzger D, and Robine S (2004). Tissue-specific and inducible Cre-mediated recombination in the gut epithelium. Genesis 39, 186–193. [PubMed: 15282745]
86. McCombe PA, and Greer JM (2022). Effects of biological sex and pregnancy in experimental autoimmune encephalomyelitis: It's complicated. Front. Immunol 13, 1059833. [PubMed: 36518769]
87. Hooke - Contract Research - Experimental autoimmune encephalomyelitis (EAE) - Mouse EAE scoring https://hookelabs.com/services/cro/eae/MouseEAEscoring.html.
88. Zhang F-L, Chen X-W, Wang Y-F, Hu Z, Zhang W-J, Zhou B-W, Ci P-F, and Liu K-X (2023). Microbiota-derived tryptophan metabolites indole-3-lactic acid is associated with intestinal ischemia/reperfusion injury via positive regulation of YAP and Nrf2. J. Transl. Med 21, 264. [PubMed: 37072757]
89. Zhang Q, Zhao Q, Li T, Lu L, Wang F, Zhang H, Liu Z, Ma H, Zhu Q, Wang J, et al. (2023). Lactobacillus plantarum-derived indole-3-lactic acid ameliorates colorectal tumorigenesis via epigenetic regulation of CD8+ T cell immunity. Cell Metabol. 35, 943–960.e9.
90. Pino PA, and Cardona AE (2011). Isolation of brain and spinal cord mononuclear cells using percoll gradients. J. Vis. Exp 2348. 10.3791/2348. [PubMed: 21339713]
91. Tian Y, Nichols RG, Roy P, Gui W, Smith PB, Zhang J, Lin Y, Weaver V, Cai J, Patterson AD, and Cantorna MT (2018). Prebiotic effects of white button mushroom (Agaricus bisporus) feeding on succinate and intestinal gluconeogenesis in C57BL/6 mice. J. Funct.Foods 45, 223–232.
92. Tian Y, Cai J, Gui W, Nichols RG, Koo I, Zhang J, Anitha M, and Patterson AD (2019). Berberine Directly Affects the Gut Microbiota to Promote Intestinal Farnesoid X Receptor Activation. Drug Metab. Dispos 47, 86–93. [PubMed: 30409838]
93. Caporaso JG, Lauber CL, Walters WA, Berg-Lyons D, Lozupone CA, Turnbaugh PJ, Fierer N, and Knight R (2011). Global patterns of 16S rRNA diversity at a depth of millions of sequences per sample. Proc. Natl. Acad. Sci. USA 108, 4516–4522. [PubMed: 20534432]
94. Bisanz J. (2024). MicrobeR: Handy tools for Microbiome analysis in R (Github). https://github.com/jbisanz/MicrobeR.
95. Palarea-Albaladejo J, and Martín-Fernández JA (2015). zCompositions – R package for multivariate imputation of left-censored data under a compositional approach. Chemometr. Intell. Lab. Syst 143, 85–96.
96. Oksanen J, Simpson GL, Blanchet FG, Kindt R, Legendre P, Minchin PR, O'Hara RB, Solymos P, Stevens MHH, Szoecs E, et al. (2024). vegan: Community Ecology Package. https://github.com/vegandevs/vegan.
97. Yu G, Smith DK, Zhu H, Guan Y, and Lam TT-Y (2017). Ggtree: An r package for visualization and annotation of phylogenetic trees with their covariates and other associated data. Methods Ecol. Evol 8, 28–36.
98. Piawah S, Kyaw TS,Trepka K, Stewart AL, Mora RV, Stanfield D, Levine K, Van Blarigan EL, Venook A, Turnbaugh PJ, et al. (2023). Associations between the Gut Microbiota, Race, and Ethnicity of Patients with Colorectal Cancer: A Pilot and Feasibility Study. Cancers 15, 4546. 10.3390/cancers15184546. [PubMed: 37760515]
99. Pinheiro J, Bates D, Debroy S, Sarkar D, EISPACK authors; Heisterkamp S., Van Willigen B, and Ranke J; R Core Team (2024). Nlme: nonlinear mixed-effects models. R package 3. https://cran.r-project.org/web/packages/nlme/nlme.pdf.

Highlights

- Ketogenic diets rescue neuroinflammation in a microbiota-dependent manner
- The diet-induced host metabolite β-hydroxybutyrate (βHB) is necessary and sufficient
- Transfer of the βHB-associated microbiota protects against neuroinflammation
- Gut bacterial indole lactate contributes to these neuroprotective effects

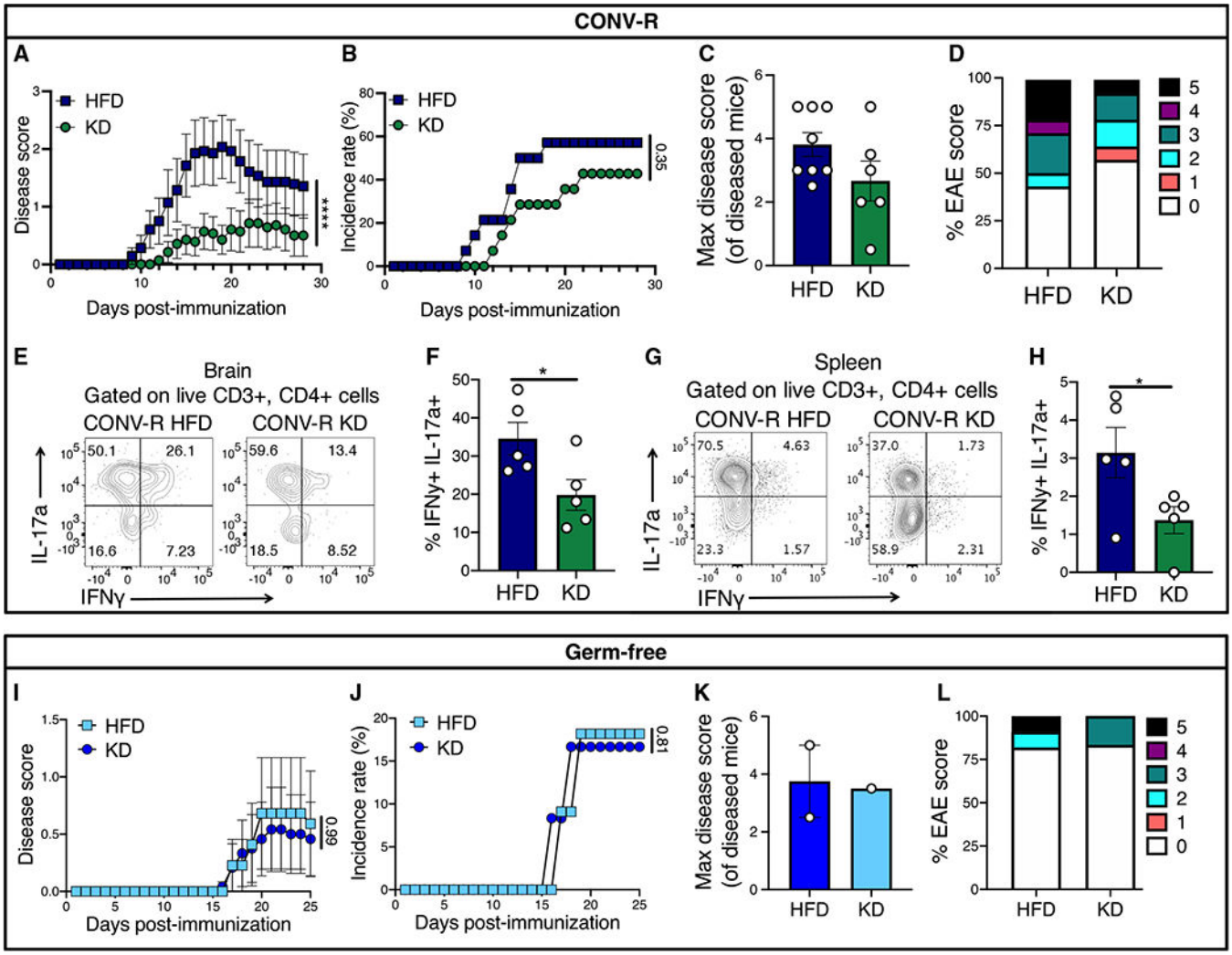

Figure 1. A ketogenic diet rescues a mouse model of multiple sclerosis in a microbiota-dependent manner

(A–D) Conventionally raised (CONV-R), specific pathogen-free, female C57BL/6J mice were fed a high-fat diet (HFD) or a ketogenic diet (KD) (Table S1) for 10 days prior to induction of the experimental autoimmune encephalomyelitis (EAE) mouse model of multiple sclerosis (n = 14/group; two independent experiments). (A) Disease scores (two-way ANOVA; mean ± SEM) and (B) disease incidence (log-rank Mantel-Cox test; percentage) were tracked over 28 days. (C) Mean disease severity of mice that develop disease (mean ± SEM; each point represents an individual mouse). (D) The proportion of mice with maximum disease score after 28 days.

(E–H) At day 16 post immunization, mice fed an HFD or KD for 4 days prior to EAE induction (n = 5/group) were sacrificed, and brain and splenic lymphocytes were profiled for T helper subsets. (E) Representative flow cytometry from brain lymphocytes of IL-17a and IFNγ cells within the live $CD3^+$ $CD4^+$ population. (F) Percentage of IL-$17a^+$ IFNγ^+ cells within the live $CD3^+$ $CD4^+$ population in the brain (Welch's t test; mean ± SEM; each point represents an individual mouse). (G) Representative flow cytometry from splenocytes of IL-17a and IFNγ cells within the live $CD3^+$ $CD4^+$ population. (H) Percentage of IL-$17a^+$

IFNγ^+ cells within the live $CD3^+$ $CD4^+$ population in the spleen (Welch's t test; mean ± SEM; each point represents an individual mouse).

(I-L) Germ-free (GF) female C57BL/6J mice were fed an HFD or KD for 7 or 16 days before EAE was induced and (I) disease scores (p value listed; two-way ANOVA; mean ± SEM) and (J) incidence rates (p value listed; log-rank Mantel-Cox test; percentage) were tracked for 25 days post immunization (n = 11 HFD; n = 12 KD; two independent experiments). (K) Mean maximum disease severity of mice that developed disease (mean ± SEM; each point represents a diseased mouse). (L) The proportion of mice with maximum disease score after 25 days.

p value listed; *$p < 0.05$; ****$p < 0.0001$.

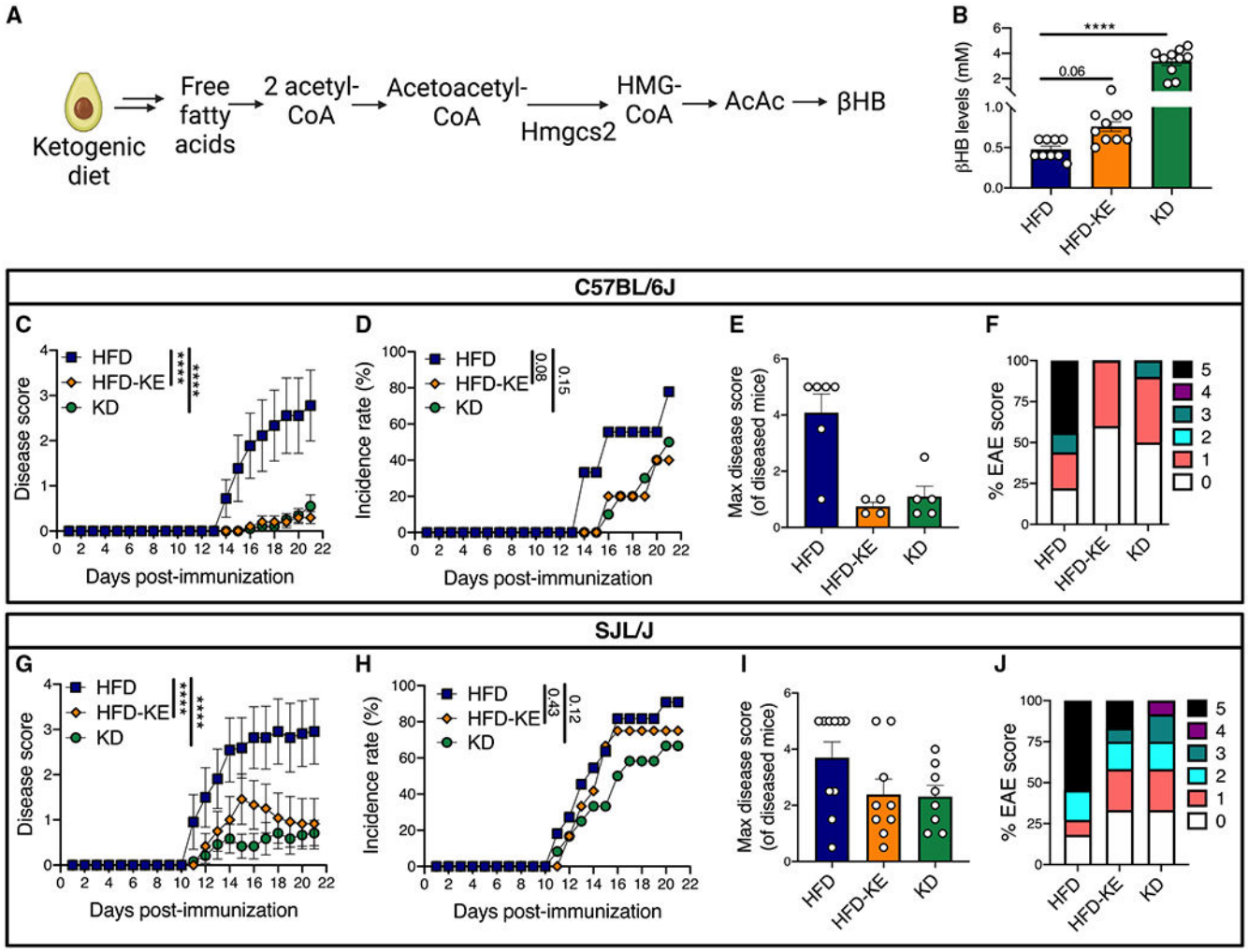

Figure 2. Oral βHB is sufficient for protection from neurological disease

(A) Pathway for β-hydroxybutyrate (βHB) production where 3-hydroxy-3-methylglutaryl-CoA synthase 2 (Hmgcs2) is the rate-limiting enzyme (AcAc, acetoacetate).

(B–F) Conventionally raised (CONV-R), specific pathogen-free, male and female C57BL/6J mice were fed a high-fat diet (HFD), an HFD supplemented with a βHB ketone ester (HFD-KE), or a ketogenic diet (KD) for 3 days prior to EAE disease induction (Table S1, n = 9 HFD; n = 10 HFD-KE and KD). (B) Circulating βHB levels 7 days post immunization. (C) Disease scores (two-way ANOVA; mean ± SEM) and (D) disease incidence (p value listed; log-rank Mantel-Cox test; percentage) was tracked over 21 days post immunization. (E) Mean maximum disease severity of mice that developed disease (mean ± SEM; each point represents a diseased mouse). (F) The proportion of mice with maximum disease score after 21 days.

(G–J) Conventionally raised (CONV-R), specific pathogen-free, female SJL/J mice were fed an HFD, HFD-KE, or a KD for 5 days prior to EAE disease induction (n = 11 HFD; n = 12 HFD-KE and KD). (G) Disease scores (two-way ANOVA; mean ± SEM) and (H) disease incidence (log-rank Mantel-Cox test; percentage) was tracked over 21 days. (I) Mean maximum disease severity of mice that developed disease (mean ± SEM; each point

represents a diseased mouse). (J) The proportion of mice with maximum disease score after 21 days.

p value listed; ****$p < 0.0001$.

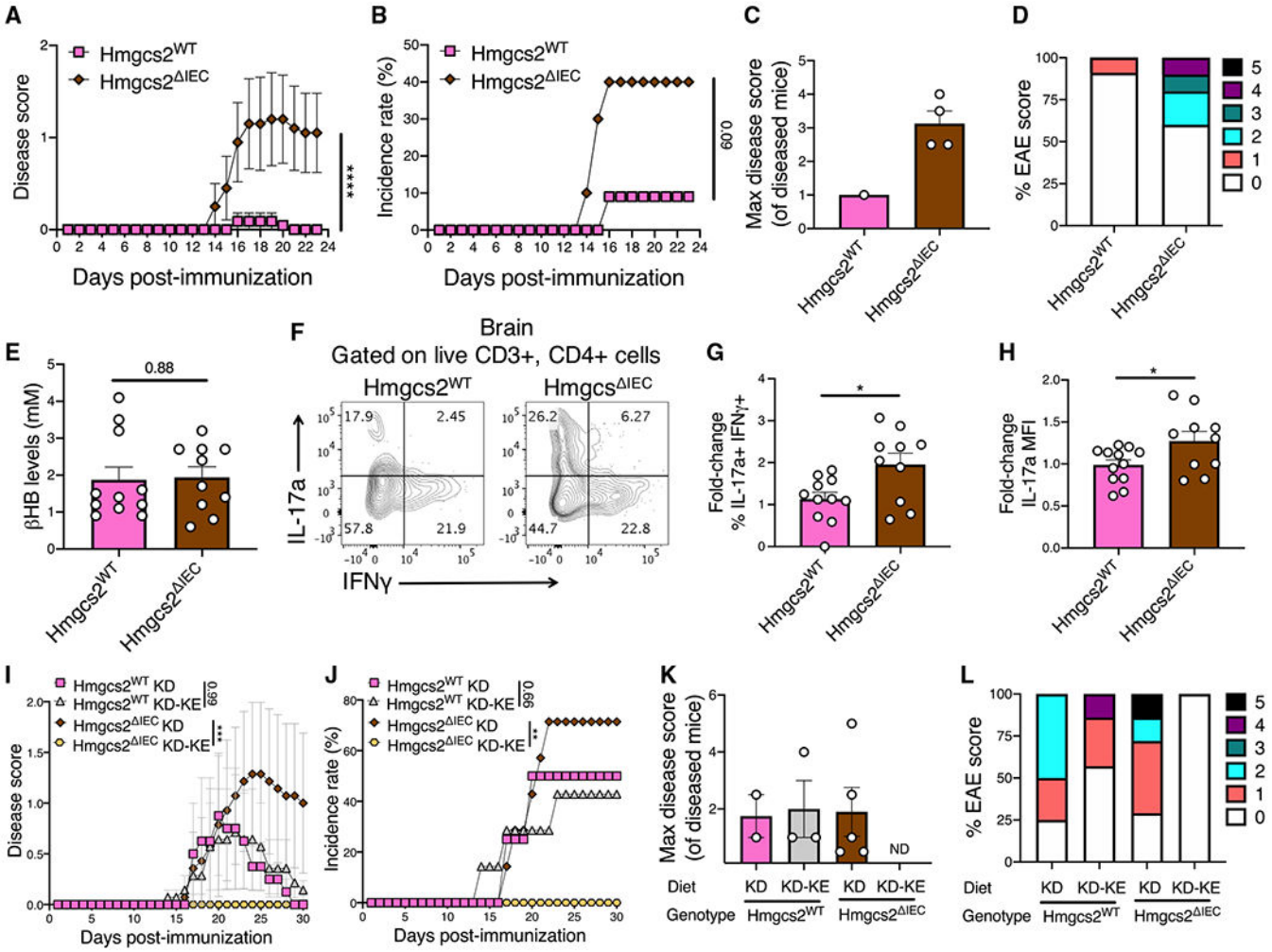

Figure 3. Intestinal βHB is necessary for protection from neurological disease

(A–H) Male *Hmgcs2*^{WT} (*Hmgcs2*$^{fl/fl}$ *VillinER/Cre*$^{-/-}$) and mice with *Hmgcs2* specifically deleted from intestinal epithelial cells (IECs) (*Hmgcs2*$^{\Delta IEC}$ – *Hmgcs2*$^{fl/fl}$ *VillinER/Cre*$^{+/-}$) were injected with tamoxifen daily for 5 days in induced *Hmgcs2* deletion. Mice then had a washout period of 5 days before being given a ketogenic diet (KD) for 3 days before EAE was induced (n = 11 *Hmgcs2*^{WT}; n = 10 *Hmgcs2*$^{\Delta IEC}$; two independent experiments).

(A–E) (A) Disease scores (two-way ANOVA; mean ± SEM) and (B) disease incidence (p value listed; log-rank Mantel-Cox test; percentage) was tracked for 23 days. (C) Mean maximum disease severity of mice that developed disease (mean ± SEM; each point represents a diseased mouse). (D) The proportion of mice with maximum disease score after 23 days. (E) Circulating βHB levels 7 days post immunization.

(F–H) Levels of Th17 cells in the brain were quantified with flow cytometry at day 23 post immunization. (F) Representative flow cytometry from brain lymphocytes of Th17 cells (IL-17a$^+$ IFNγ$^+$ cells within the live CD3$^+$ CD4$^+$ population). (G) Fold change relative to the *Hmgcs2*^{WT} group in the IL-17a$^+$ IFNγ$^+$ cells within the live CD3$^+$ CD4$^+$ population and (H) IL-17a mean fluorescence intensity within the live TCRβ$^+$ population (Welch's t test; mean ± SEM; each point represents an individual mouse).

(I–L) Male *Hmgcs2*^{WT} (*Hmgcs2*$^{fl/fl}$ *VillinER/Cre*$^{-/-}$) or *Hmgcs2*$^{\Delta IEC}$ (*Hmgcs2*$^{fl/fl}$ *VillinER/Cre*$^{+/-}$) were injected with tamoxifen daily for 5 days, after which the mice had a washout period of 5 days before being put on a KD or a KD supplemented with a βHB ketone ester (KD-KE) (Table S1) for 5 days before EAE was induced ($n = 4$ *Hmgcs2*^{WT} KD; $n = 7$ *Hmgcs2*^{WT} KD-KE, *Hmgcs2*$^{\Delta IEC}$ KD, and *Hmgcs2*$^{\Delta IEC}$ KD-KE). (I) Disease scores (two-way ANOVA; mean ± SEM) and (J) disease incidence rates (log-rank Mantel-Cox test; percentage) were tracked for 30 days. (K) Mean maximum disease severity of mice that developed disease (mean ± SEM; each point represents a diseased mouse; ND, not detected). (L) The proportion of mice with maximum disease score after 30 days.
p value listed; *$p < 0.05$; **$p < 0.01$; ***$p < 0.001$; ****$p < 0.0001$.

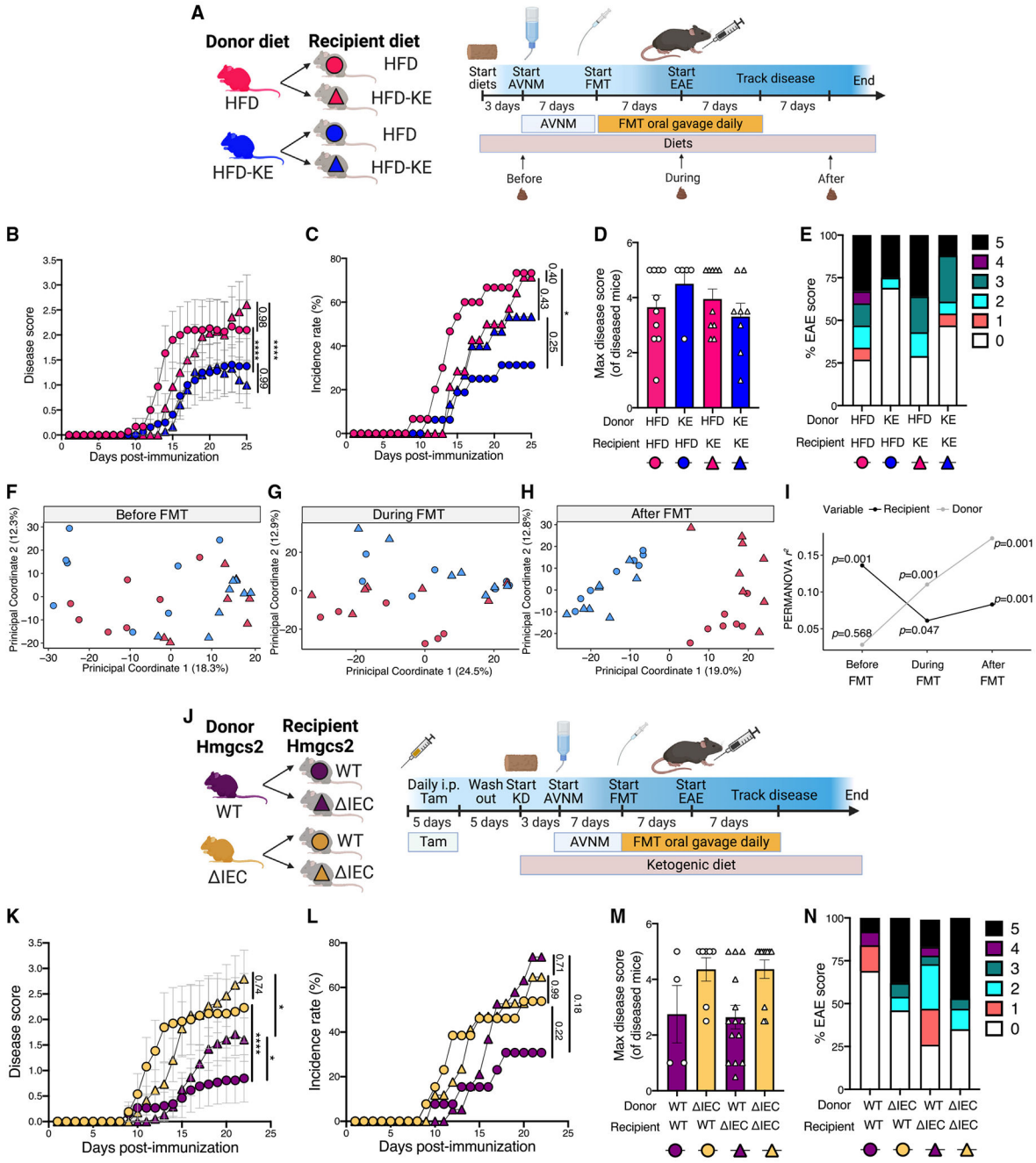

Figure 4. The βHB-altered gut microbiota is sufficient to protect from disease

(A–I) Fecal microbiota transplantation (FMT) experiments between mice fed a high-fat diet (HFD) or HFD + βHD ketone ester (HFD-KE). HFD or HFD-KE donor fecal microbiota were transplanted into AVNM-treated HFD- or HFD-KE-fed recipients before EAE was induced (n = 15 HFD microbiota to HFD recipient, pink circles; n = 14 HFD microbiota to HFD-KE recipient, pink triangles; n = 16 HFD-KE microbiota to HFD recipient, blue circles; n = 15 HFD-KE microbiota to HFD-KE recipient, blue triangles; two independent

experiments). Time points for fecal sample collection for 16S-seq are indicated on the timeline.

(A–E) (A) Experimental design and timeline for diet FMT experiments. (B) Disease scores (two-way ANOVA; mean ± SEM) and (C) disease incidence rates (log-rank Mantel-Cox test; percentage) were tracked over 25 days post immunization. (D) Mean disease severity of mice that developed disease (mean ± SEM; each point represents a diseased mouse). (E) The proportion of mice with maximum disease score after 25 days.

(F–I) Principal coordinate analysis of Euclidean distances (F) before, (G) during, and (H) after FMTs. (I) PERMANOVA testing of recipient (black) and donor (gray) diet before, during, or after FMTs.

(J–N) *Hmgcs2*^{WT} or *Hmgcs2*$^{\Delta IEC}$ fecal microbiota was transplanted into KD-fed AVNM-treated *Hmgcs2*^{WT} and *Hmgcs2*$^{\Delta IEC}$ recipient mice before EAE was induced ($n = 13$ *Hmgcs2*^{WT} microbiota to *Hmgcs2*^{WT} recipient, purple circles; $n = 13$ *Hmgcs2*$^{\Delta IEC}$ microbiota to *Hmgcs2*^{WT} recipient, yellow circles; $n = 19$ *Hmgcs2*^{WT} microbiota to *Hmgcs2*$^{\Delta IEC}$ recipient, purple triangles; $n = 17$ *Hmgcs2*$^{\Delta IEC}$ microbiota to *Hmgcs2*$^{\Delta IEC}$ recipient, yellow triangles). (J) Experimental design and timeline. (K) Disease scores (two-way ANOVA; mean ± SEM) and (L) disease incidence rates (log-rank Mantel-Cox test; percentage) were tracked over 22 days. (M) Mean disease severity of mice that developed disease (mean ± SEM; each point represents a diseased mouse). (N) The proportion of mice with maximum disease score after 22 days.

p value listed; *$p < 0.05$; ****$p < 0.0001$.

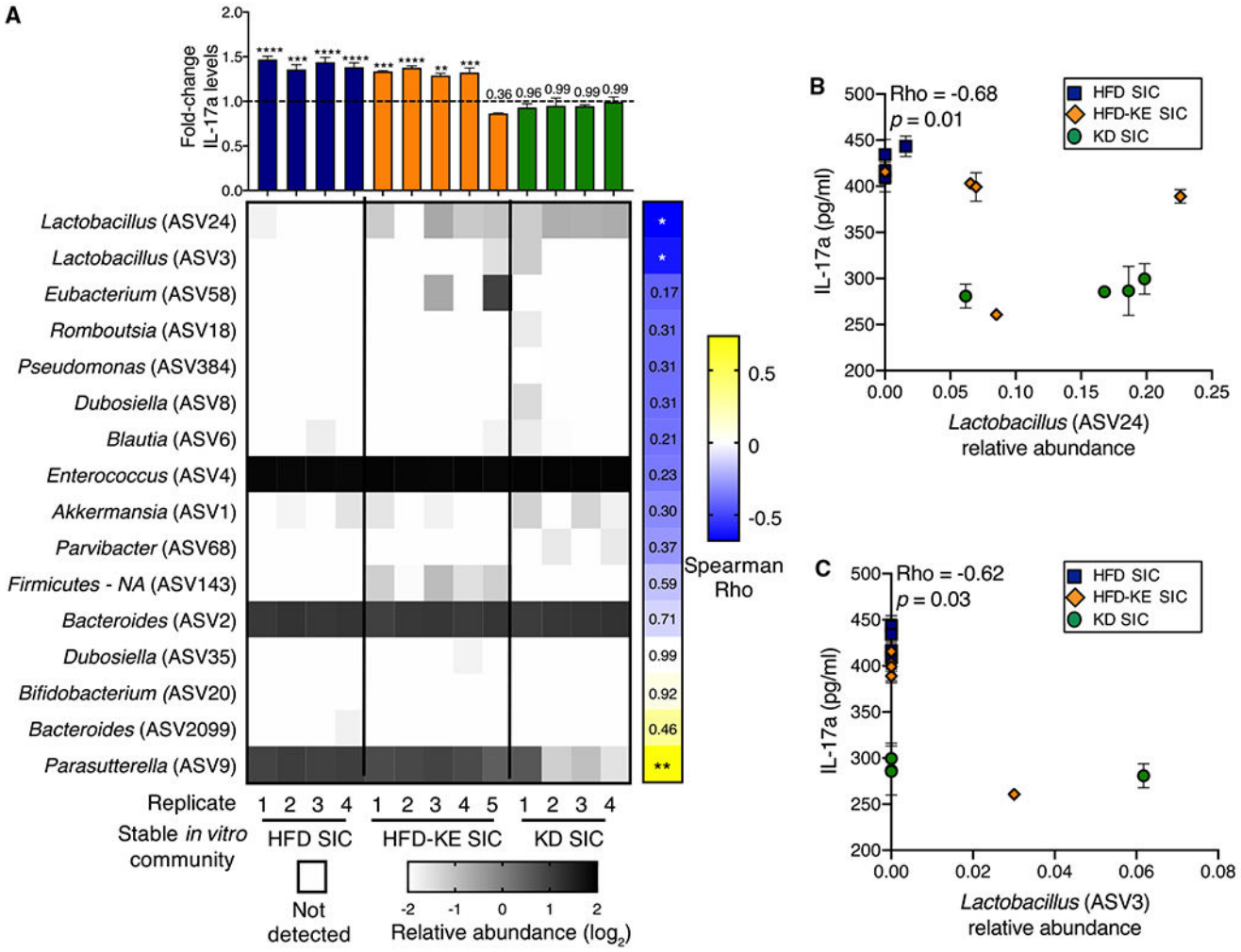

Figure 5. *Lactobacillus* sequence variants are associated with decreased Th17 activation

(A–C) Stool stable *in vitro* communities (SICs) were derived from high-fat diet (HFD), HFD supplemented with a βHB ketone ester (HFD-KE), or a ketogenic diet (KD) mouse stool 7 days post EAE induction (1 donor/group, 4–5 SIC replicates). SIC cell-free supernatants (CFSs) were tested in a Th17 skewing assay, and community structure was assessed with 16S rRNA gene sequencing.

(A) (Top) IL-17a levels were measured via ELISA post restimulation of Th17 skewed splenic T cells treated with CFSs from HFD-, HFD-KE-, and KD EAE-derived SICs where cells were treated for 4 days ($n = 3$ for Th17 skewing biological replicates, one-way ANOVA with Dunnett's multiple comparisons test compared to BHI medium control; fold change is relative to the BHI medium control, which is represented by the dotted line; mean ± SEM). (Bottom) Heatmap of the relative abundance (log_2) of amplicon sequence variants (ASVs) in the SICs with assigned genus (SILVA v.138 database). White denotes the absence of an ASV. (Right) Spearman correlation Rho values of ASV relative abundance and IL-17a levels (Spearman correlation).

(B and C) Significantly negatively correlated ASVs with IL-17a levels, (B) ASV24 and (C) ASV3, from the Spearman correlation of ASV relative abundance and IL-17a levels are

plotted in individual scatterplots (Spearman correlation; mean ± SEM). p value listed; *p < 0.05; **p < 0.01; ***p < 0.001; ****p < 0.0001.

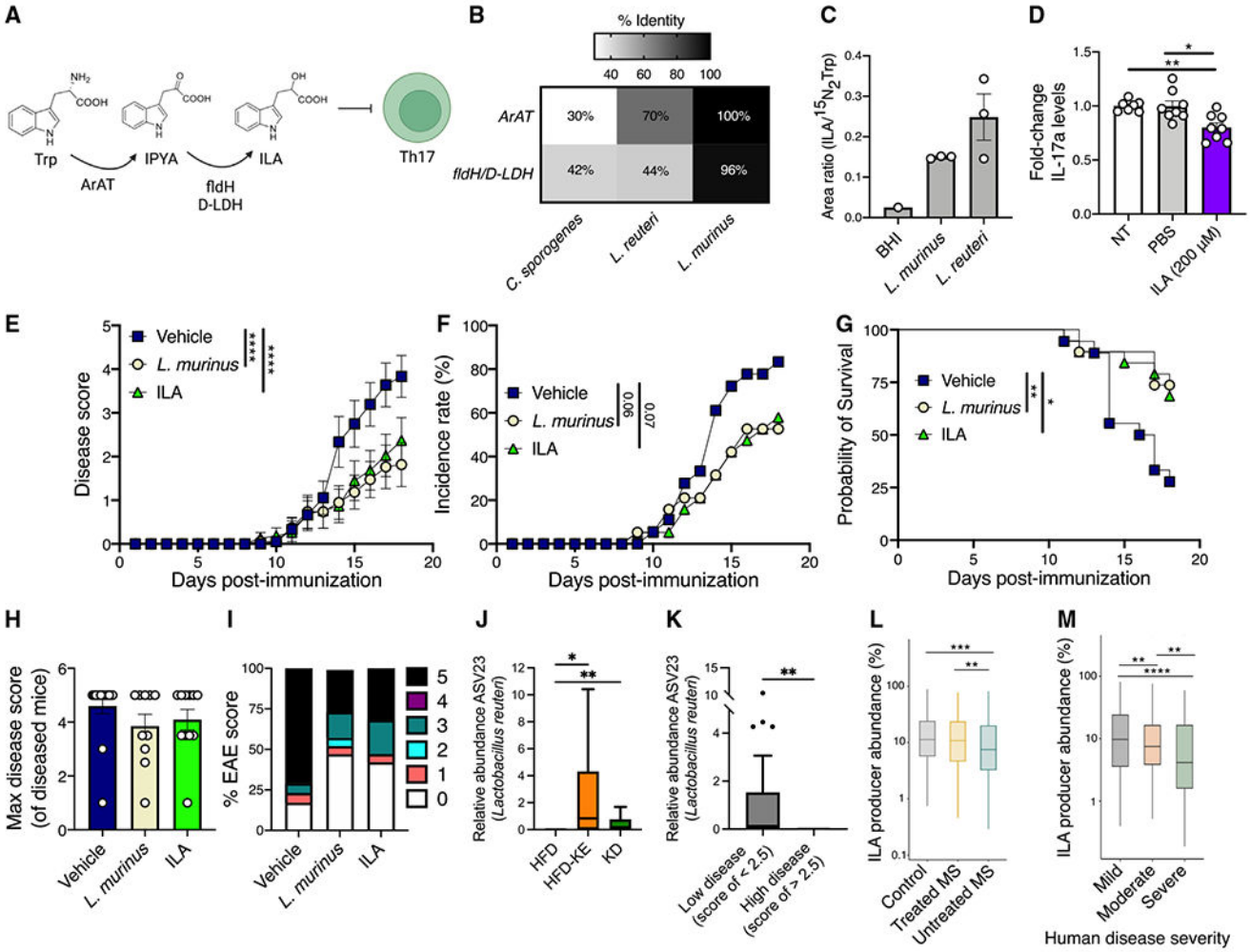

Figure 6. A *Lactobacillus murinus* isolate and metabolite decrease disease severity on an HFD

(A) Tryptophan (Trp) metabolism pathway where Trp is metabolized to indole-3-pyruvate (IPYA) via aromatic aminotransferase and is then metabolized to ILA via indolelactate dehydrogenase (fldH) or lactate dehydrogenase (LDH). ILA can inhibit Th17 cells.[51]

(B) Top hits in the *L. murinus* KD6 genome for ArAT and D-LDH with percent identity (listed) and compared to *Clostridium sporogenes, L. reuteri,* and *L. murinus* via BLASTP (E value <1e–51). See also Tables S4 and S5.

(C) ILA was quantified via high-resolution liquid chromatography-mass spectrometry from *L. murinus* KD6 or *L. reuteri* strain ATCC23272 cultured in BHI^{CHV}. The area ratio of ILA to labeled Trp ($^{15}N_2$ Trp) is displayed (n = 3 biological replicates *L. murinus* KD6 and *L. reuteri; n* = 1 for BHI control; mean ± SEM).

(D) IL-17a levels in Th17 skewed cells that were incubated for 4 days with no treatment (NT), a vehicle control (PBS), or 200 μM indole-3-lactate (ILA) post restimulation (n = 7–8; each point represents a Th17 biological replicate one-way ANOVA Kruskal-Wallis with Dunn's test; mean ± SEM; values are relative to NT; two independent experiments).

(E–I) CONV-R specific pathogen-free female C57BL/6J mice were fed a high-fat diet (HFD) for 3 days prior to the start of oral gavage every other day with PBS, *L. murinus*

KD6, or indole-3-lactate (ILA). EAE was induced 4 days later (n = 18 vehicle [PBS]; n = 19 *L. murinus;* n = 19 ILA; mean ± SEM; two independent experiments). (E) Disease scores (two-way ANOVA; mean ± SEM), (F) disease incidence rates (log-rank Mantel-Cox test; percentage), and (G) survival (log-rank Mantel-Cox test; percentage) were tracked over 18 days post immunization. (H) Mean disease severity of mice that developed disease (mean ± SEM; each point represents a diseased mouse). (I) Proportion of mice with maximum disease score after 18 days.

(J) Relative abundance of ASV24 *L. reuteri* in mice fed HFD, HFD-KE, or KD 7 days post EAE induction as quantified by 16S-seq (related to Figures 2 and S5; n = 9–10; Kruskal-Wallis with Dunn's test; Tukey box-and-whisker plot).

(K) Relative abundance of ASV24 *L. reuteri* in mice with no or mild disease (EAE score of <2.5; n = 32) and mice with severe disease (score of >2.5; n = 5; Welch's t tests; Tukey box-and-whisker plot).

(L) Relative abundance of ILA-producing bacteria in control (n = 576), treated (n = 367), and untreated (n = 209) MS subjects (unpaired Wilcoxon tests).

(M) Relative abundance of ILA-producing bacteria in MS subjects with mild, moderate, and severe disease. Mild: EDSS 0–3.5, no severe disability/highly ambulatory (n = 414); moderate: EDSS 4–6.5, severe disability while still ambulatory (n = 140); severe: EDSS 7–9.5, wheelchair bound (n = 21, unpaired Wilcoxon tests).

p value listed; *p < 0.05; **p < 0.01; ***p < 0.001; ****p < 0.0001.

KEY RESOURCES TABLE

REAGENT or RESOURCE	SOURCE	IDENTIFIER
Antibodies		
CD3; Clone: 17a2; Fluorophore: FITC	Fisher Scientific	Cat: 501129303 RRID: AB_2621660
IL-17a; Clone: ebio17b7; Fluorophore: PE-Cyanine7	Fisher Scientific	Cat: 501129407 RRID: AB_2534297
CD4; Clone: GK1.5; Fluorophore: BV786	Fisher Scientific	Cat: BDB563331 RRID: AB_2738140
IFNy; Clone: XMG1.2; Fluorophore: BV421	Fisher Scientific	Cat: BDB563376 RRID: B_2738165
TCRbeta; Clone: H57-597; Fluorophore: PE-CF594	Fisher Scientific	Cat: BDB562841 RRID: AB_2565655
anti-CD3e	Fisher Scientific	Cat: BDB553057 RRID: AB_394590
anti-CD28	Fisher Scientific	Cat: BDB557393 RRID: AB_396676
anti-IFNy	Fisher Scientific	Cat: BDB554409 RRID: AB_398550
anti-IL4	Fisher Scientific	Cat: 5013602 RRID: AB_468410
Rabbit anti-mHMGCS2	Santa Cruz Biotechnology Inc.	Cat. sc-393256; RRID: AB_3662814
Mouse anti-mGAPDH	Prointech	Cat. 60004; RRID: AB_2919886
Goat anti-rabbit IgG	Southern Biotech	Cat. 4030-05; RRID: AB_609686
Goat Anti-Mouse IgG	Abcam	Cat. Ab6708; RRID: AB_956005
Bacterial and virus strains		
Lactobacillus murinus strain KD6	Turnbaugh Lab	This study
Chemicals, peptides, and recombinant proteins		
Fetal Bovine Serum, heat inactivated	Life technologies	Cat: 10438026
Sodium Pyruvate (100 mM)	Life technologies	Cat: 11360070
Penicillin-Streptomycin (5,000 U/mL)	Thermo Fisher	Cat: 15070063
MEM Non-Essential Amino Acids	Life technologies	Cat: 11140050
GlutaMAX	Gibco	Cat: 35050061
Bacto Brain Heart Infusion (BHI) (broth)	Fisher Scientific	Cat: 237500
L-Cysteine	Sigma Aldrich	Cat: W326305
Resazurin	Fisher Scientific	Cat: 199303-5G
Hemin, 5G	Fisher Scientific	Cat: 51280-5G
Menadione (Vitamin K)	Fisher Scientific	Cat: 102259
IL-6	VWR	Cat: 575704-BL
TGFβ	Fisher Scientific	Cat: 7666-MB-005
Cell stimulation cocktail	Fisher Scientific	Cat: 501129036
Golgi plug	Fisher Scientific	Cat: BDB555029
Ampicillin	Millipore Sigma	Cat. A9393

REAGENT or RESOURCE	SOURCE	IDENTIFIER
Neomycin	Sigma Aldrich	Cat. N5285
Metronidazole	Sigma Aldrich	Cat. M1547
Vancomycin	Sigma Aldrich	Cat. V1130
MOG peptide: $pMOG_{35–55}$	Tocris	Cat: 25681
Heat-killed Mycobacterium tuberculosis (MTB)	Fisher Scientific	Cat: DF3114338
Incomplete Freund's adjuvant	Millipore Sigma	Cat: F5506
Pertussis toxin	Millipore Sigma	Cat: P7208
Difco Lactobacilli MRS agar	BD biosciences	Cat: 288210
1X Phosphate-buffered saline (PBS), pH 7.4	Thermo Fisher	Cat: 10010023
Percoll Density Gradient Media	VWR	Cat: 89428-524
Hank's balanced Salt Solution (HBSS) - no calcium no magnesium, no phenol red	Life Technologies	Cat: 14170161
Hydroxyethyl piperazineethanesulfonic acid (HEPES)	Fisher Scientific	Cat: NC0734307
Ethylenediaminetetraacetic acid (EDTA)	Fisher Scientific	Cat: AM9260G
DL-Dithiothreitol (DTT)	VWR	Cat: 97063-760
Tamoxifen	Sigma	Cat: T5648
Corn oil	Fisher Scientific	Cat: S25271
$PLP_{139–151}$	Genscript	Custom synthesis with >95% purity by HPLC and <10EU/mg endotoxin, sequence: HSLGKWLGHPDKF [unmodified]
DL-Indole-3-lactic acid	Sigma	Cat: I5508
3-Hydroxybutyric acid (βHB)	Sigma	Cat: 166898
Hexanoyl hexyl β-hydroxybutyrate (C6x2-BHB) ester (ketone ester - KE)	BHB Therapeutics	N/A
Critical commercial assays		
LIVE/DEAD Fixable Dead Cell Stain Kit - aqua	Fisher Scientific	Cat: 501121526
Fixation/Permeabilization Solution Kit	Fisher Scientific	Cat: BDB555028
IL-17A (homodimer) Mouse Uncoated ELISA Kit	Fisher Scientific	Cat: 5017377
ZymoBIOMICS 96 MagBead DNA Kit	Zymo Reseach	Cat: D4302/D4306/D4308
Syber select	Life Technologies	Cat: 4472908
RBC lysis buffer	Fisher Scientific	Cat: NC9067514
Dynabeads untouched mouse CD4 cells	ThermoFisher	Cat: 11415D
Deposited data		
16S-seq	NCBI	Bioproject: PRJNA1032118
L. murinus KD6 whole genome sequence	NCBI	Bioproject: PRJNA1032118
Experimental models: Organisms/strains		
Wildtype C57BL/6J mice	Jackson Labs	Cat: 000664
Hmgcs2fl/fl VillinER/Cre+/−	Turnbaugh Lab	This study
Hmgcs2fl/fl VillinER/Cre−/−	Turnbaugh Lab	This study
Wildtype SJL/J mice	Jackson Labs	Cat: 000686

REAGENT or RESOURCE	SOURCE	IDENTIFIER
Oligonucleotides		
V4-515F:	IDT	5’ TCGTCGGCAGCGTCAGATGTGTATAAG AGACAGGTGCCAGCMGCCGCGGTAA 3’
V4-806R:	IDT	5’ GTCTCGTGGGCTCGGAGATGTGTATAA GAGACAGGGACTACHVGGGTWTCTAAT 3’
VillinER/Cre F	IDT	5’ TTC CCG CAG AAC CTG AAG ATG 3’
VillinER/Cre R	IDT	5’ CCC CAG AAA TGC CAG ATT ACG 3’
HMGCS2 F	IDT	5’ GTG AGT TCT GTG CCT GAC TG 3’
HMGCS2 R	IDT	5’ CAG AGC TGC AAG ATG AGT AAC TG 3’
Software and algorithms		
GraphPad Prism 8	GraphPad Software	https://www.graphpad.com/
FlowJo v10.6.1	TreeStar	https://www.flowjo.com/
R 3.4.0	R	https://r-project.org
QIIME2	Bolyen et al.[74]	https://qiime2.org/
SILVA v138 database	Quast et al. [75]	https://www.arb-silva.de/documentation/release-138/
ALDEx2	Gloor et al.[76]	https://www.bioconductor.org/packages/release/bioc/html/ALDEx2.html
DADA2 v1.8.0	Callahan et al. [77]	https://benjjneb.github.io/dada2/
Porechop v0.2.4	Wick[78]	https://github.com/rrwick/Porechop
Flye v2.9.2	Kolmogorov et al. [79]	
Pilon v1.24	Walker, Bruce et al. [80]	https://doi.org/10.1371/journal.pone.0112963
Bakta v1.8.1	Schwengers et al. [81]	
Circulator v1.5.5	Hunt et al. [82]	
Quast v5.2.0	Gurevich et al. [83]	
Growthcurver v0.3.1	Sprouffske & Wagner[84]	
Other		
Mouse diet: Standard chow diet SPF, CONV-R mice	Lab diet	Cat: 5058
Mouse diet: Standard autoclaved chow diet (germ-free studies)	Lab diet	Cat: 5021
High-fat diet (75% kcal fat, HFD)	Envigo	TD.160239
Ketogenic Diet (44% Crisco, 15% CocB, 8.5% CO)	Envigo	TD.160153
C6x2-BHB HFD (10%, 75/Fat, Crisco, CocB, CO)	Envigo	TD.170411
C6x2-BHB Ketogenic Diet (10%, Crisco, CocB, CO)	Envigo	TD.170411